# Phase transitions in InSb at pressures up to 5 GPa

R. J. Nelmes, M. I. McMahon, P. D. Hatton, J. Crain, and R. O. Piltz

*Department of Physics, The University of Edinburgh, Mayfield Road, Edinburgh, EH9 3JZ, United Kingdom*

(Received 29 June 1992; revised manuscript received 17 September 1992)

The structural phase transitions in InSb at pressures up to 5 GPa at room temperature have been reexamined by angle-dispersive powder-diffraction techniques on a synchrotron source using an image-plate area detector. Two distinct behaviors have been found: (1) the cubic zinc-blende phase ($P1$) transforms at $\sim 2.1$ GPa to a mixture of a tetragonal phase ($P2$) and an orthorhombic phase ($P3$), which then transforms to nearly single-phase $P3$ before recrystallizing to another orthorhombic phase ($P4$) at the same or only a slightly higher pressure; or (2) $P1$ transforms directly to $P4$ at $\sim 3.0$ GPa. $P2$ is previously unobserved at room temperature. It has a $\beta$-tin structure (but it is *not* the InSb-II phase) and appears not to be long-range site ordered. $P3$ is the InSb-II phase, which is now shown to be orthorhombic and site ordered. $P4$ is the InSb-IV phase, but it is shown to have many previously unobserved superlattice reflections. $P4$ is also site ordered. The three phases $P2$, $P3$, and $P4$ appear to account for all previous clear results on InSb at room temperature in this pressure range, and it is shown that the long-accepted $P$-$T$ phase diagram is incorrect.

## I. INTRODUCTION

Among group IV and III-V semiconductors, indium antimonide has been one of the most extensively studied under pressure. However, significant uncertainties remain about the crystal structures of the high-pressure phases. As summarized below, the literature contains several examples of less than satisfactory fits between observed and calculated powder patterns, and some instances where observed powder patterns could not be interpreted at all. And in all cases it has not been possible to discover whether the high-pressure structures are site ordered, because the difference in scattering between In and Sb has been too small to detect.

Under ambient conditions InSb has the cubic zinc-blende structure. A transition from this under pressure was first reported by Gebbie et al.[1] but attributed to melting. Jayaraman et al.[2] showed that the transition was to a solid phase, and detected a volume decrease (or density increase) of about 20% near 2 GPa at room temperature. They designated the high-pressure form as phase II and, by analogy with the isoelectronic element tin, suggested that the structure would be the diatomic analogue of $\beta$-tin. Subsequent diffraction studies appeared to confirm this, with a transition at 2.3 GPa and tetragonal unit-cell dimensions $a = b = 5.79$ Å and $c = 3.11$ Å measured at 2.5 GPa.[3-6] Then Kasper and Brandhorst[7] found a different behavior. They obtained no transition until they reached a significantly higher pressure of $\sim 3.0$ GPa where the cubic phase transformed to a simple orthorhombic structure with $a = 2.92$ Å, $b = 5.56$ Å, and $c = 3.06$ Å. This unit cell contains two atoms, at $(0,0,0)$ and $(0, \frac{1}{2}, \alpha \sim \frac{1}{2})$, and the density is the same as phase II within experimental uncertainties. The new phase was subsequently designated as phase IV. Its discovery raised the question as to which was the equilibrium high-pressure phase. McWhan and

Marezio[8] found that they obtained InSb II if pressure was raised rapidly through the transition and InSb IV if it was raised gradually. Later, this was interpreted[9] as showing InSb II to be the equilibrium phase just above room temperature, on the basis that passing rapidly through the transition would heat the sample; once in phase II the transition to the true room-temperature equilibrium phase (IV) would be very sluggish.[9]

These results were consolidated into the generally accepted $P$-$T$ phase diagram of InSb by Banus and Lavine.[9] They drew together earlier high-temperature work of their own and others,[2,5,6,10,11] and made further extensive studies of the boundaries between phases II and IV, and between them and the phase designated III found at high-temperatures (above 575 K at 3 GPa) and high pressures (above 9 GPa at room temperature). They located the II-III-IV triple point at 6.5 GPa and 450 K. This work made extensive use of recovered phases, obtained by quenching to $\sim 80$ K before releasing the pressure. Earlier, Darnell and Libby[12] had shown that this procedure, starting from about 2.5 GPa and 370 K, yields a hard, machinable metal which remains stable for weeks provided that it is kept below 210 K. The powder pattern from this material corresponds very closely to that of the $\beta$-tin structure. These results were reproduced and confirmed in further work by Darnell and Libby[13] and others,[6-8,14,15] and it was generally assumed that the recovered phase and InSb II were one and the same. Certainly this was taken to be an established fact by Banus and Lavine[9] in mapping out the field of InSb II in the $P$-$T$ phase diagram, though Kasper and Brandhorst[7] had expressed doubts about $\beta$-tin being the correct structure for InSb II, and McWhan and Marezio[8] had shown that InSb IV also recovers to the $\beta$-tin phase at 77 K and atmospheric pressure.

A decade later, Yu et al.[16] attempted to obtain more accurate results for the crystal structures of InSb II, III,

© 1993 The American Physical Society

and IV. In the case of InSb IV, they confirmed the ortho-rhombic structure obtained by Kasper and Brandhorst[7] but found $\alpha$, the $z$ coordinate of the second atomic site, to be $\sim\frac{1}{4}$ rather than $\frac{1}{2}$ and concluded that the space group of the structure is $Pmm2$. Based on the phase diagram of Banus and Lavine,[9] they then attempted to heat the sample into phase II, but obtained a pattern they could not index or interpret. Degtyareva et al.[17] made a systematic study of the effects of small composition variations on the phases found in quenched samples. Starting from 3.8 GPa and 175 °C with a 50:50 sample they obtained the or-thorhombic pattern of InSb IV rather than $\beta$-tin. This and other results led the authors to suggest that the $P$-$T$ phase diagram needed to be substantially revised. Most recently, Vanderborgh et al.[18] have studied the room-temperature structural transitions in InSb up to 66 GPa, using energy-dispersive techniques on a synchrotron source. The transition from the cubic to orthorhombic phase (IV) first started at 2.8 GPa and required a further slight increase in pressure to complete. The best fit to their InSb IV powder pattern was obtained with the same structure as Yu et al.[16] but with $\alpha=0.38$. However, they note that this had been shown to be an energetically un-favorable structure[19] because each atom has four (out of six) nearest neighbors the same as itself (assuming a site-ordered structure). Although, as in all the previous work, they were not able to show the structure to be site ordered, they hypothesised that it is and that the true unit cell is doubled along the $a$ and $c$ axes of the $Pmm2$ cell. This allows a NaCl-like structure with alternate (010) NaCl planes displaced $a/2$ (in the enlarged cell) along the $c$ axis; each atom then has six unlike nearest neighbors. On increasing pressure above 6 GPa, they ob-served changes in the diffraction pattern, including peaks they could not index. They attributed this to a transition to a new phase (InSb V) which gradually becomes more hexagonal with further increase of pressure, until the transition to (hexagonal) InSb III is complete at 17.5 GPa. Then InSb III transforms to a bcc structure (CsCl if ordered) at 28 GPa, which remains up to the highest pressure reached (66 GPa).[18]

The appearance of phase V in the supposedly well-established field of phase IV, and the inability of Yu et al.[16] to find phase II, underline the doubts about the $P$-$T$ phase diagram of InSb raised by Degtyareva et al.[17] Also, there is clear evidence in the published literature that InSb II does not have the $\beta$-tin structure. The second pair of strong lines in the $\beta$-tin powder pattern, (220) and (211), should have a separation in scattering an-gle ($2\theta$) about $\frac{2}{3}$ that of the first pair, (200) and (101). But all the reported patterns[3,5,7,8] have the (220) reflection missing—as remarked by Kasper and Brandhorst.[7] The photograph of InSb at 2.5 GPa published by Hanneman et al.[6] shows that this line should be resolvable; in fact the $2\theta$ separation of (220) and (211) in $\beta$-tin is very simi-lar to that of (120) and (111) in InSb IV which are readily resolved.[7,8] The more extended patterns[8,9] show up fur-ther significant discrepancies in higher-angle lines. This poor fit is remarked upon by McWhan and Marezio.[8] (It is worth noting that their pattern from the recovered $\beta$-tin phase at 1 atm and 77 K does not have these prob-

lems.[8]) In the case of Banus and Lavine,[9] the mis-fits are obscured only because they index half their lines as reflections not allowed by the $\beta$-tin structure.

There is a clear need to reexamine the crystallography of the high-pressure phases of InSb using techniques with higher resolution and sensitivity. We are now carrying out a systematic study using angle-dispersive x-ray diffraction on a synchrotron source. In this paper we present our first results, which focus principally on the phases found at room temperature up to 5 GPa. We show that phase II has an orthorhombic structure, and that the structure of phase IV is much more complex than previously supposed. We also find a phase with the $\beta$-tin structure appearing at room temperature (in addition to phase II). And we have been able to determine the site ordering of all three structures. Be-cause our results suggest that the phase diagram of InSb has to be substantially revised, we do not use the labels II and IV for the structures we have found since these labels refer to $P$-$T$ fields of stability we would now question.

## II. EXPERIMENTAL TECHNIQUES

The x-ray diffraction data were collected on station 9.1 at SRS, Daresbury, using angle-dispersive techniques and an image-plate detector. A water-cooled channel-cut Si(111) monochromator was used to select the required wavelength ($\sim 0.45$ Å) from the spectrum of the 5-T wiggler magnet. Tests showed that the proportion of $\lambda/3$ (and higher order) component in the incident beam at $\lambda \sim 0.45$ Å is too small to detect in a powder pattern. Considerable care was taken to eliminate other possible contaminant features in the powder patterns (gasket lines, for example) and to minimize the background level. The two-dimensional powder patterns recorded on the image plate were integrated (around the powder rings) to give conventional 1D profiles. Figure 1(a) shows a pattern recorded at a sample to image-plate distance of 250 mm, and the corresponding integrated profile is in Fig. 1(b). The inset shows the wealth of information obtained even at the highest scattering angles. Details of our beamline set-up, experimental procedures, and pattern integration have been published separately.[20−23] They are develop-ments of the image-plate techniques pioneered at the Photon Factory for angle-dispersive x-ray powder diffraction at high pressure.[24]

We used both Merrill-Bassett[25] and Diacell[26] diamond-anvil cells (DAC's), which have full conical apertures of half angle $\geq 40°$. Samples of InSb were prepared from two different sources, one with a purity $>99.99\%$ and another $>99.9999\%$. Finely ground powder was loaded into the DAC's, with a 4:1 mixture of methanol and ethanol as the pressure transmitting medi-um. The diameter of the sample chamber was in the range 150–250 $\mu$m, and the incident x-ray beam was col-limated to a diameter not exceeding half this size. Small chips of ruby were enclosed with the sample so that the pressure could be measured by the ruby fluorescence technique.[27]

The absolute incident x-ray wavelength was calibrated by carrying out a conventional $2\theta$ scan of a standard powder sample of Si and fitting to the measured peak po-

sitions. Small changes in the wavelength from this cali-brated value were then calculated from the accompany-ing change in monochromator angle (varied in such a way as to eliminate backlash errors). For work very close to the In $K$ edge, the edge was first located from the vari-ation of absorption with incident wavelength using a sample of (cubic) InSb at ambient pressure, and then the monochromator was offset the required amount.

Integration of the 2D patterns requires an accurate measurement of the dimensions of the pixels forming the image, and must take account of any deviation of the im-age plate from being perpendicular to the primary beam. And to derive a powder profile as a function of $2\theta$, it is also necessary to know the distance from the sample to the image plate accurately. Our procedures for meeting these requirements are described in Refs. 20 and 21. It should be added that measurements of the sample-to-plate distance neglected any variation of this distance with pressure due to compression of the sample; but the effect of this will be small, and less than other sources of error. The structural results given in this paper were all obtained by full Rietveld refinement[28] of the integrated profiles, using the program MPROF.[29]

## III. RESULTS AND ANALYSIS

First we present the bare, reproducible facts of the transition from the cubic phase at room temperature, as
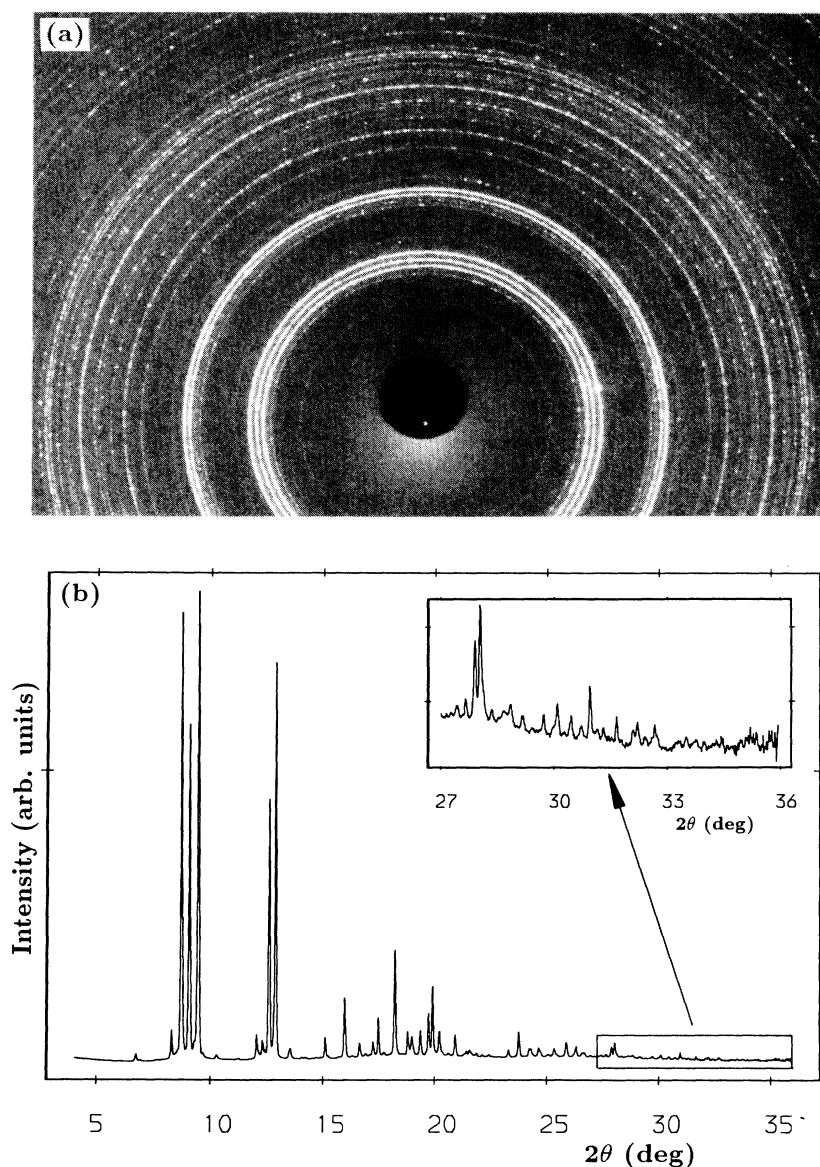


FIG. 1. (a) A full two-dimensional powder pattern recorded from InSb at a sample-to-plate distance of 250 mm, using an incident wavelength of 0.4446 Å. The sample was held in a Merrill-Bassett diamond-anvil cell at ~2.5 GPa. Exposure time was 84 min. (b) The corresponding integrated profile. The high-angle part of the profile is enlarged in the inset.

we have found them. Subsequently we explain how these findings relate to previous work. This is discussed further in Sec. IV, along with other related results from our work.

We find two distinct sequences when the pressure is increased gradually, in small steps, involving four phases—the cubic zinc-blende phase (phase 1 or $P1$), a tetragonal phase ($P2$), and two orthorhombic phases ($P3$ and $P4$).

### Sequence (a)

At ~2.1 GPa the cubic phase begins to transform, as shown in Fig. 2. The region of the pattern enlarged in the inset reveals three new lines (arrowed) just emerging, alongside the very weak (200) reflection from the cubic phase. With a slight tightening of the pressure cell, all of the cubic phase transforms (Fig. 3); we have never observed anything near a 50:50 mixture of these cubic and high-pressure phases. (This "slight tightening" of the cell would be equivalent to a pressure increase of 0.1–0.2 GPa in the absence of any discontinuous behavior of the sample. However, the volume collapse when the cubic phase transforms to a high-pressure phase causes a reduction in the sample pressure, and in that case it is probable that this tightening is simply maintaining the pressure rather than increasing it further.) Examination of Fig. 3 shows that the pattern is from a mixture of two phases. In both the 2D image and the integrated profile, the first strong line [at $2\theta = 8.72°$, and marked by the arrow in Fig. 3(a)] is clearly sharper than the two lines next to it; similar features can be found at higher $2\theta$, as marked by asterisks in Fig. 3(b). The broad lines are from the tetrag-



FIG. 2. The integrated profile of a pattern recorded from cubic InSb at ~2.1 GPa, showing the first appearance of lines of the high-pressure phases, $P2$ and $P3$, as enlarged and labeled 1, 2, 3 in the inset. The first three strong lines of the cubic phase are indexed. The inset also shows the very weak (200) reflection of the cubic phase, which arises from the difference in scattering between In and Sb.

onal phase $P2$, which is the dominant phase in this pattern, and the sharp lines are from the orthorhombic phase $P3$. The inset in Fig. 3(b) shows the first three strong lines on the same $2\theta$ scale as the inset in Fig. 2. The relative intensities and positions of the peaks, and also the relative proportions of the two phases, appear to have remained almost constant throughout the transition.

On a further slight tightening of the pressure cell (as described above), $P3$ becomes dominant, but with a significant component of $P2$ remaining. Over the following $\frac{1}{2}$ to 1 h, without any measurable change in pressure, the $P2$ component reduces further (by transformation to $P3$), to a level of about 5% as shown in Fig. 4. This level of $P2$ remains indefinitely. There are two visible $P2$ lines which do not overlap with $P3$ lines. They are both marked with arrows in Fig. 4(b), and the lower angle one [line 2 of Fig. 3(b)] is a distinct feature of the 2D image, as labeled "a" in Fig. 4(a). Other $P2$ lines show up as a widening of the base of $P3$ peaks [e.g., as marked $\Delta$ in Fig. 4(b)] or as broad shoulders on $P3$ peaks [marked ∗ in inset (i) of Fig. 4(b)]. The mixing of the phases is illustrated further in Fig. 5 which shows calculated patterns for pure $P3$ and $P2$, one above the other, and (inset) mixed patterns with $P2$ dominating and with $P3$ dominating. (These patterns are taken from the fit discussed later in relation to Fig. 10.) The arrows and asterisks mark the peaks in the $P2$ pattern responsible for the features marked by the same symbols in Fig. 4(b). And the peaks labeled with asterisks under the $P3$ pattern account for the sharp peaks indicated in Fig. 3(b).

After a longer time of several hours, again without any change in pressure (from just above 2.1 GPa), spots appear in the 2D image as shown in Fig. 6(a). The smooth lines are from $P3$ [as in Fig. 4(a)]; this phase is recrystallizing to a second orthorhombic phase ($P4$) giving the spotty lines. [$P2$ is still present, as shown by the broad low-angle line, marked "a"—the same line as "a" in Fig. 4(a).] The $P4$ lines are much more numerous: many of them lie almost exactly on $P3$ lines; but a few $P3$ lines are not overlapped [as labeled "b" in Fig. 6(a), for example]. These features suggest that $P4$ has a larger unit cell that is related in some simple way to the $P3$ cell. The $P3$ to $P4$ transformation continues with time until the population of the $P4$ lines becomes high enough to make them appear almost continuous. But even after several weeks the process does not proceed beyond a roughly equal mix of $P3$ and $P4$. The typical end point of this first sequence is thus a three-phase mixture containing a few percent of $P2$.

The integrated profile in Fig. 6(b) reveals a weak low-angle line for $P4$, close to that of $P3$ [inset (i)]. This $P3$ line is thus one of those not overlapped by a $P4$ line; others are marked by asterisks in Fig. 6(b), corresponding to the lines labeled "b" in Fig. 6(a).

If pressure is increased on the $P2$-$P3$-$P4$ mixture at any stage, none of the components appears to grow at the expense of the others up to at least 5 GPa: the mixture simply compresses. A special case of this is seen if pressure is increased above ~3 GPa as soon as the $P2$ to $P3$ transition has taken place. The pattern then remains as in Fig. 4, and $P4$ does not appear.
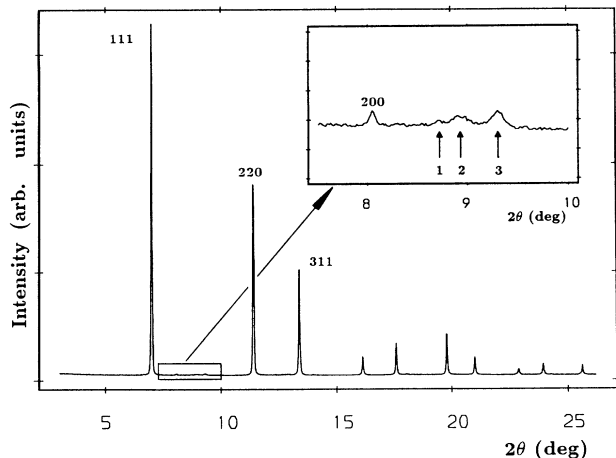
### Sequence (b)

Sometimes no transition is observed at ~2.1 GPa, and the pressure is gradually increased to ~3 GPa before the cubic phase starts to transform directly to $P4$ (Fig. 7). Comparison with Fig. 2 reveals that the cubic-phase lines are broader than at the start of the transition to $P2$-$P3$. The first five strongest $P4$ lines are marked with asterisks in insets (i) and (ii) of Fig. 7 [compare inset (ii) of Fig. 6(b)]. Inset (i) also shows the very weak (200) reflection of the cubic phase. With maintenance of pressure, more of the cubic phase transforms [Fig. 7 insets (iii) and (iv)] and proceeds continuously to completion (Fig. 8)—i.e., unlike sequence (a) where we only ever observe the cubic phase dominating (Fig. 2) or almost entirely transformed (Fig. 3).

A reproducible characteristic of this direct transformation of cubic to $P4$ is that, as shown in Fig. 8(a), the lines do *not* have the spotty nature seen in Fig. 6(a); this accords with $P4$ being produced directly from a pulverizing transition rather than by recrystallization as in sequence (a). Also, the relative intensities of the lines [Fig. 8(b)]
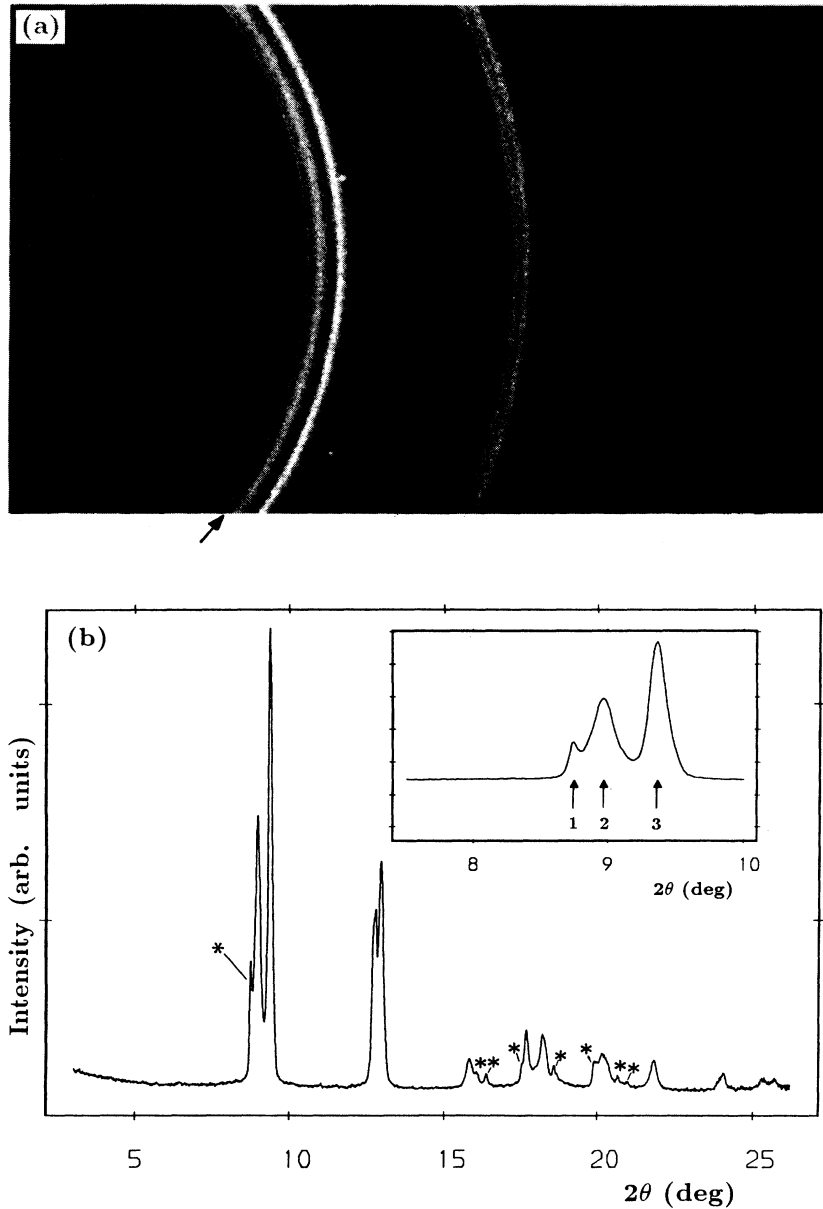


FIG. 3. (a) A pattern recorded from a mixture of InSb $P2$ and $P3$ at, or slightly above, the pressure in Fig. 2. The arrow marks the first line of one phase ($P3$). The adjacent broader lines are the first two of the second phase ($P2$). $\lambda=0.4442$ Å. Exposure time = 10 min. Sample-to-plate distance = 350 mm. (b) The corresponding integrated profile. The asterisks mark the sharp-peaked features of $P3$. The inset displays the first three peaks on the same $2\theta$ scale as in the inset of Fig. 2.

are significantly different from those found in sequence (a) [see inset (ii) of Fig. 6(b)], and we will suggest that this is because the direct transition gives rise to significant preferred orientation whereas reaching $P4$ via recrystallization from $P3$ does not. It can be seen that the relative intensities at the very beginning of the transition [insets (i) and (ii) of Fig. 7] are the same as at its completion [Fig. 8(b)]. A third interesting characteristic of the direct transition is the apparent jump in lattice parameters as the last of the cubic phase transforms. This can be seen in the relative position of the middle peak of the low-angled triplet in the insets of Fig. 7 compared with its position in Fig. 8(b).

The arrow under the main profile in Fig. 8(b) marks a very weak $P3$ (or possibly $P2$) line. At no stage in the transition sequence (b) is this ever anything more than a very minor component (see also the insets of Fig. 7). The probable origin of this component is discussed later.

### Heating

It is useful to present one other observation at this stage. We carried out an experiment in which the cubic-phase sample was heated to 100 °C and then the pressure
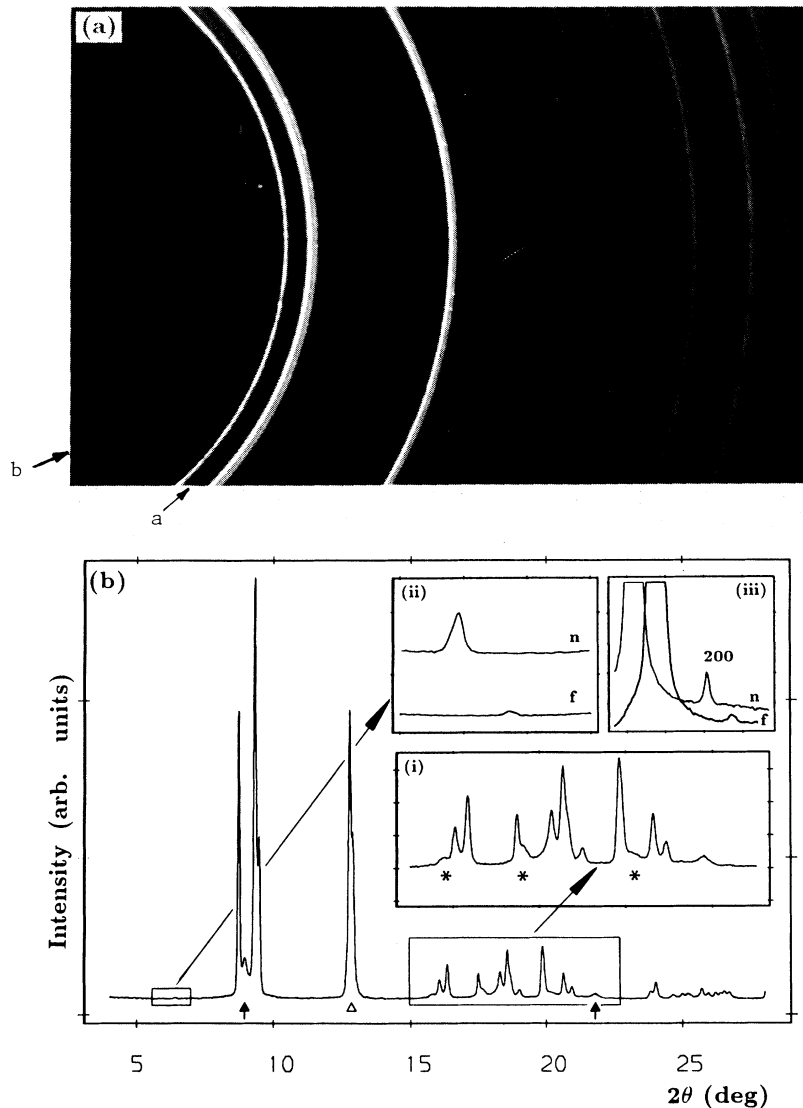


FIG. 4. (a) A pattern recorded from a mixture of InSb $P2$ and $P3$ at, or slightly above, $\sim 2.1$ GPa. The lowest-angle strong line of $P2$ is labeled "a" and the very weak low-angle line of $P3$ is labeled "b." $\lambda = 0.4446$ Å. Exposure time = 14 min. Sample-to-plate distance = 250 mm. (b) The corresponding integrated profile. The arrows below the profile mark the two nonoverlapped $P2$ lines (the one at $2\theta \sim 9°$ is marked "a" in the 2D pattern). The features marked $\Delta$ and * [inset (i)] are discussed in the text. Inset (ii) shows the very weak low-angle line of $P3$ (marked "b" in the 2D pattern) recorded with an incident energy of 25.83 keV, far ($f$) from the In $K$ edge (as in the main profile), and at 27.886 keV near ($n$) the In $K$ edge (at 27.925 keV). Inset (iii) shows the cubic (200) reflection recorded with the same two incident x-ray energies as for inset (ii).
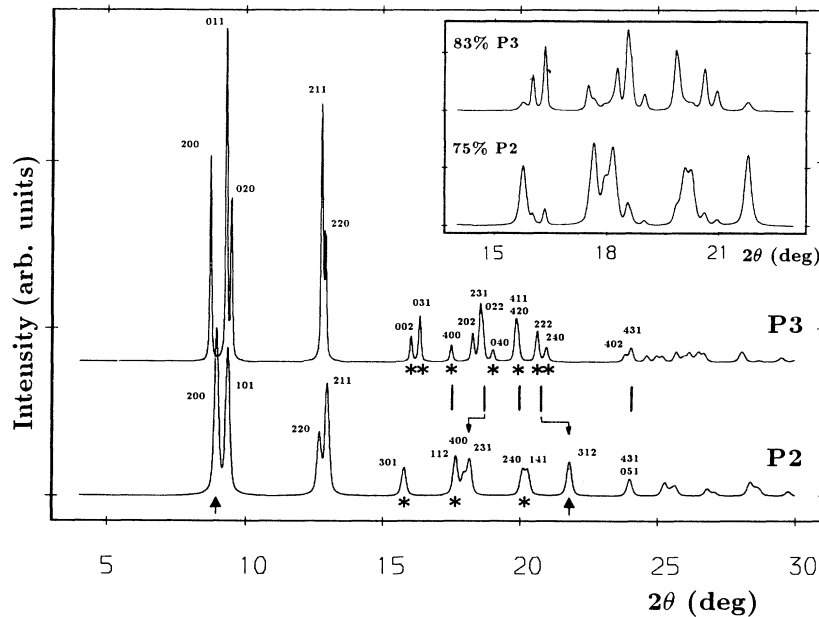
FIG. 5. The calculated and indexed profiles for InSb $P2$ and $P3$. The arrows and asterisks under the $P2$ profile mark the peaks responsible for the features marked by the same symbols in Fig. 4(b). The asterisks under the $P3$ profile mark the peaks giving the sharp features labeled ( * ) in Fig. 3(b). The lower profile in the inset is a mixture of these calculated profiles with mostly (75%) $P2$ for comparison with Fig. 3(b), and the upper profile is mostly (83%) $P3$ for comparison with the inset (i) of Fig. 4(b). The bars between the two main profiles are the positions of the lines observed by McWhan and Marezio (Ref. 8) in this $2\theta$ range. Their $\beta$-tin indexing is shown ⌐—⌐ and ⌐—⌐ where a significant displacement is involved.

was increased (still at 100 °C). We obtained the almost entirely "clean" $P4$ pattern shown in Fig. 9(a). The lines are "spotty" in character [compare Fig. 8(a)], and the intensity distribution [Fig. 9(b)] is the same as in inset (ii) of Fig. 6(b). We therefore suggest that the elevated temperature has brought about a complete transformation to $P4$ by sequence (a)—i.e., by recrystallization from $P3$. As already noted we were not able to achieve this at room temperature.

We are now in a position to discuss the three high-pressure phases $P2$, $P3$, and $P4$ in more detail, and relate them to previous work.

### Tetragonal $P2$

The $d$ spacings and relative intensities of the broad lines of Fig. 3 correspond closely to a $\beta$-tin structure with unit cell dimensions $a = 5.697(1)$ Å and $c = 3.104(1)$ Å, obtained by Rietveld refinement. *We should stress immediately that this is not the InSb II phase,* which is clearly *not* tetragonal (as previously reported) but orthorhombic as discussed under $P3$ below.

Figure 10 shows the fit to the profile in Fig. 3(b) obtained with a multiphase Rietveld refinement which simultaneously models the broad $P2$ pattern and the sharp $P3$ component. We have found that a significant improvement in fit is obtained if $P2$ is refined with anisotropic peak widths—the ($h00$) lines appearing to be wider than other $P2$ lines. [Note, however, that only the (200) and (400) lines from $P2$ are present in the pattern

shown in Fig. 10, and that, as seen in Fig. 5, the (400) line is overlapped by the (112) and (231) lines of $P2$.] Observed and calculated $d$ spacings for $P2$ are given in Table I. One observed value (marked * ) is displaced due to overlap with $P3$ peaks.

The inset in Fig. 10 shows the positions of the $P2$ and $P3$ (110) reflections, and the observed profile (crosses) in this region. Above that are the calculated profiles (i) if $P2$ is disordered and $P3$ is ordered (labeled "do") and (ii) if both are ordered (labeled "oo"). The integrated intensity of the combined peak in the "oo" profile is five times as large as in "do" because the sample contains approximately four times as much $P2$ as $P3$. As shown in the next section, $P3$ *is* site ordered, and there is some evidence of a very weak feature at the correct position in the observed profile. But the larger peak centered over the $P2$ position, required if $P2$ is ordered, does not seem to be observed. Although the level of noise in the data leaves a little room for doubt, we conclude that $P2$ is very probably not long-range site ordered.

As already outlined, when the high-pressure phases of InSb above 2.1 GPa are cooled to 77 K at pressure, and then decompressed to ambient pressure, a true $\beta$-tin phase (*not* the same as InSb II) is obtained.[12,13] It seems possible that we have detected the same phase occurring at room temperature.

It is unsurprising that $P2$ has not been observed before. Figure 4(b) shows that once $P3$ is formed there are only two nonoverlapped $P2$ lines, even with the pattern resolution of synchrotron angle-dispersive techniques, and

the lines are very weak. Then the pattern in Fig. 3 was obtained only after these extra lines had been identified in the $P3$ pattern [as in Fig. 4(b)], and it required several repeated efforts knowing what we were looking for.

### Orthorhombic $P3$

All the lines of the $P3$ pattern can be indexed on an orthorhombic unit cell with $a = 5.847(1)$ Å, $b = 5.388(1)$

Å, and $c = 3.181(1)$ Å. This orthorhombic pattern has been reported previously in quenched samples, but not interpreted.[17] The lowest-angle line of the $P3$ pattern is very weak; it can be just discerned at "b" in Fig. 4(a). Inset (ii) in Fig. 4(b) shows this line as recorded at an incident x-ray wavelength of $\sim 0.48$ Å, far ($f$) from the In $K$-absorption edge (as for the main profile), and near ($n$) the edge at a wavelength of 0.4446 Å. (The wavelength change shows up in the small shift of the line to lower



FIG. 6. (a) A pattern recorded from a sample of InSb $P3$ partly transformed to $P4$ just above 2.1 GPa. Some $P2$ is also still present, as shown by the line labeled "a." The $P3$ lines labeled "b" are not overlapped by any $P4$ lines, and hence are free from spots. $\lambda = 0.4446$ Å. Exposure $= 10$ min. Sample-to-plate distance $= 250$ mm. (b) The corresponding integrated profile. Asterisks mark the strongest of the nonoverlapped $P3$ lines, labeled "b" in (a). The low-angle weak line of $P3$ is enlarged in inset (i), with a weak $P4$ line alongside. Inset (ii) shows the part of the profile below $2\theta = 15°$, with the best-fitting calculated $P3$ profile subtracted to reveal the main $P4$ lines.

TABLE I. Observed and calculated d spacings ($d_0$ and $d_c$), refined unit-cell dimensions and unit-cell volumes for phases P2, P3, and P4 (subcell and true cell)) of InSb at ~2.3 GPa at room temperature. Values of $d_0$ are determined to ±0.002 Å in P2 and ±0.001 Å in P3 and P4. Very weak lines are omitted. In the case of P4, only the reflections indexable on the subcell (as $hkl_s$) are included; their true indices for the full unit cell ($hkl$) are also given. Under P2, the asterisk marks a reflection displaced in position by overlap with a P3 line, and "nr" denotes reflections not resolved in the mixed P2-P3 profile. $N_A$ is the number of atoms in the unit cell.

| P2 | | | P3 | | | P4 | | | |
|---|---|---|---|---|---|---|---|---|---|
| $hkl$ | $d_0$(Å) | $d_c$(Å) | $hkl$ | $d_0$(Å) | $d_c$(Å) | $hkl_s$ | $hkl$ | $d_0$(Å) | $d_c$(Å) |
| 200 | 2.850 | 2.848 | 110 | 3.962 | 3.964 | 001 | 002 | 3.064 | 3.068 |
| 101 | 2.728 | 2.725 | 200 | 2.924 | 2.924 | 100 | 200 | 2.923 | 2.925 |
| 220 | 2.010 | 2.014 | 011 | 2.739 | 2.739 | 020 | 060 | 2.810 | 2.809 |
| 211 | 1.974* | 1.969 | 020 | 2.693 | 2.694 | 011 | 032 | 2.691 | 2.692 |
| 301 | 1.618 | 1.620 | 211 | 2.002 | 1.998 | 101 | 202 | 2.116 | 2.117 |
| 112 | 1.448 | 1.448 | 220 | 1.982 | 1.981 | 021 | 062 | 2.071 | 2.071 |
| 400 | nr | 1.424 | 002 | 1.592 | 1.591 | 120 | 260 | 2.027 | 2.026 |
| 231 | 1.406 | 1.408 | 031 | 1.563 | 1.564 | 111 | 232 | 1.981 | 1.981 |
| 240 | 1.272 | 1.274 | 400 | 1.462 | 1.462 | 121 | 262 | 1.691 | 1.691 |
| 141 | nr | 1.262 | 202 | 1.398 | 1.397 | 031 | 092 | 1.599 | 1.598 |
| 312 | 1.176 | 1.176 | 231 | 1.379 | 1.379 | 002 | 004 | 1.533 | 1.534 |
| 431/051 | 1.068 | 1.070 | 022 | 1.371 | 1.370 | 012 | 034 | 1.480 | 1.479 |
| 103/332 | 1.016 | 1.018/1.016 | 040 | 1.345 | 1.347 | 200 | 400 | 1.463 | 1.463 |
| 440/531 | 1.001 | 1.007/1.001 | 411 | 1.289 | 1.290 | 040/131 | 0120/292 | 1.404 | 1.404/1.403 |
| | | | 420 | 1.285 | 1.285 | 102 | 204 | 1.359 | 1.358 |
| | | | 222 | 1.240 | 1.240 | 022 | 064 | 1.346 | 1.346 |
| | | | 240 | 1.222 | 1.223 | 112/201 | 234/402 | 1.320 | 1.320/1.320 |
| | | | 402 | 1.076 | 1.076 | 220 | 460 | 1.298 | 1.297 |
| | | | 431 | 1.067 | 1.068 | 211 | 432 | 1.286 | 1.285 |
| | | | 013 | 1.040 | 1.040 | 140 | 2120 | 1.267 | 1.266 |
| | | | 042 | 1.026 | 1.028 | 122 | 264 | 1.224 | 1.223 |
| | | | 051 | 1.018 | 1.021 | 221 | 462 | 1.195 | 1.195 |
| | | | 422 | 0.998 | 1.000 | 032 | 094 | 1.187 | 1.186 |
| | | | 440 | 0.989 | 0.991 | 141 | 2122 | 1.172 | 1.170 |
| | | | 213 | 0.980 | 0.980 | 132 | 294 | 1.101 | 1.099 |
| | | | | | | 231 | 492 | 1.081 | 1.079 |
| | | | | | | 202 | 404 | 1.058 | 1.058 |
| | | | | | | 212 | 434 | 1.042 | 1.040 |
| | | | | | | 042 | 0124 | 1.038 | 1.036 |
| | | | | | | 003 | 006 | 1.023 | 1.022 |
| | | | | | | 240 | 4120 | 1.015 | 1.013 |
| | | | | | | 151 | 2152 | 1.008 | 1.006 |
| $a$(Å) | 5.697(1) | | | 5.847(1) | | 2.925(1) | 5.850(2) | | |
| $b$(Å) | 5.697(1) | | | 5.388(1) | | 5.617(1) | 16.851(2) | | |
| $c$(Å) | 3.104(1) | | | 3.181(1) | | 3.067(1) | 6.134(1) | | |
| $V$(Å³) | 100.72(4) | | | 100.21(4) | | 50.40(3) | 604.80(36) | | |
| $N_A$ | 4 | | | 4 | | 2 | 24 | | |

$2\theta$.) When recorded away from the In edge, the strength of this line is about 1/1000th of the strongest lines, and this is the right order of magnitude for reflections in which In and Sb scatter in antiphase—as for the cubic (200) reflection shown for comparison in inset (iii). The pronounced increase in intensity near the In $K$ edge [seen also for the cubic (200) reflection] confirms this interpretation, and the structure is thus shown to be site ordered. We believe this to be the first reported observation of anomalous-scattering effects in high-pressure powder diffraction.

Reflections with $h + k + l = $ odd are absent from the profile, showing that the structure is body centered. Also reflections with $k + l = $ odd are absent away from the In $K$ edge, apart from the (very weak) low-angle reflection (110) shown in the lower ($f$) profile of inset (ii) in Fig. 4(b). This indicates pseudo-$A$-face centering, with In at (0,0,0) and Sb at, or very near, $(0,\frac{1}{2},\frac{1}{2})$. The structure thus differs from $\beta$-tin by a displacement of the Sb atoms $\frac{1}{4}$ along $z$ relative to the In atoms, in addition to the orthorhombic distortion of the unit cell. Fuller details of the determination and refinement of the crystal structure will be published separately, but Fig. 11 shows a fit to the profile in Fig. 4(b) at the present stage of analysis. This again requires a multiphase Rietveld refinement to take
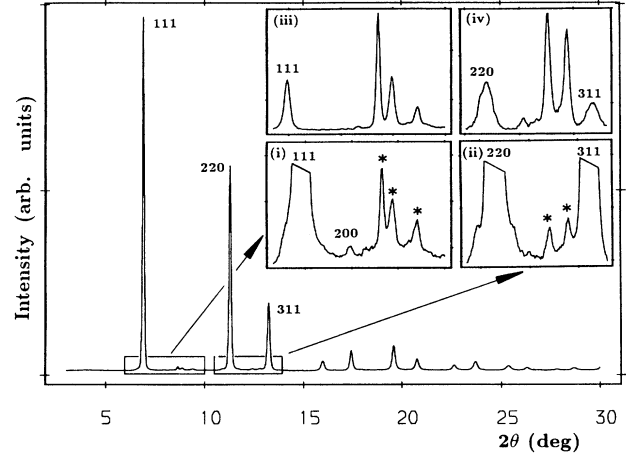


FIG. 7. The integrated profile of a pattern recorded from cubic InSb at $\sim 3$ GPa, showing the first appearance of lines of the high-pressures phase $P4$, as enlarged and marked by asterisks in insets (i) and (ii). The first three strong lines of the cubic phase are indexed. Inset (i) also shows the very weak (200) reflection of the cubic phase, which results from the difference scattering between In and Sb. Insets (iii) and (iv) show the same reflections as (i) and (ii) at a later stage of the transformation, when the cubic lines are weaker than the main $P4$ lines.

TABLE II. Observed $d$ spacings and $2\theta$ angles ($d_0$ and $2\theta_0$), and refined unit-cell dimensions for phase $P3$ of InSb at $\sim 2.3$ GPa at room temperature. The brackets in column 3 group together reflections not resolved from each other in lower-resolution or broadened patterns, such as in Fig. 12(b). In estimating the mean $2\theta_0$ values for these groups, lines have been weighted by their relative intensities. The observed $d$ spacings at 4.0 GPa published by McWhan and Marezio (Ref. 8) are included for comparison and also expressed in terms of observed $2\theta$ values ($2\theta_0$) at a common incident wavelength of 0.4446 Å, along with the calculated $2\theta$ values ($2\theta_c$) and indexing for the $\beta$-tin unit cell they adopted. The underlined values in columns 6 and 7 show the largest discrepancies of the $\beta$-tin indexing. The unit-cell dimensions for the data of McWhan and Marezio (Ref. 8) are given as re-refined on the orthorhombic cell (column 5) and as published by them for the $\beta$-tin cell (column 7). $N_A$ is the number of atoms in the unit cell.

| | Present work at 2.3 GPa | | | Ref. 8 at 4.0 GPa | | $\beta$-tin indexing | |
| --- | --- | --- | --- | --- | --- | --- | --- |
| $hkl$ | $d_0$(Å) | $2\theta_0$(°) ($\lambda=0.4446$ Å) | Mean $2\theta_0$(°) | $d_0$(Å) | $2\theta_0$(°) ($\lambda=0.4446$ Å) | $2\theta_c$(°) ($\lambda=0.4446$ Å) | $hkl$ |
| 200 | 2.924 | 8.72 | 8.72 | 2.902 | 8.79 | 8.80 | 200 |
| 011 | 2.739 | 9.31 ⎤ | 9.36 | 2.717 | 9.39 | 9.33 | 101 |
| 020 | 2.693 | 9.47 ⎦ | | | | | |
| 211 | 2.002 | 12.75 ⎤ | 12.79 | 1.983 | 12.87 | 12.46 | 220 |
| 220 | 1.982 | 12.88 ⎦ | | | | 12.84 | 211 |
| 002 | 1.592 | 16.05 ⎤ | 16.25 | | | | |
| 031 | 1.563 | 16.35 ⎦ | | | | | |
| 400 | 1.462 | 17.49 | 17.49 | 1.459 | 17.53 | 17.64 | 112 |
| 202 | 1.398 | 18.30 ⎤ | | | | 17.66 | 400 |
| 231 | 1.379 | 18.55 | 18.56 | 1.374 | 18.62 | 17.92 | 231 |
| 022 | 1.371 | 18.66 | | | | | |
| 040 | 1.345 | 19.03 ⎦ | | | | | |
| 411 | 1.289 | 19.86 ⎤ | 19.88 | 1.281 | 19.99 | 19.77 | 240 |
| 420 | 1.285 | 19.92 ⎦ | | | | 20.00 | 141 |
| 222 | 1.240 | 20.65 ⎤ | 20.75 | 1.232 | 20.79 | 21.66 | 312 |
| 240 | 1.222 | 20.96 ⎦ | | | | | |
| 402 | 1.076 | 23.85 ⎤ | 23.98 | 1.069 | 24.00 | 23.65 | 501 |
| 431 | 1.067 | 24.05 ⎦ | | | | | |
| $a$(Å) | 5.847(1) | | | 5.81(2) | | 5.79 | |
| $b$(Å) | 5.388(1) | | | 5.44(2) | | 5.79 | |
| $c$(Å) | 3.181(1) | | | 3.15(1) | | 3.10 | |
| $V$(Å$^3$) | 100.21(4) | | | 99.6(6) | | 103.9 | |
| $N_A$ | 4 | | | 4 | | 4 | |

account of the residual P2 component. The remaining mis-fits to the intensities (shown below the profile in Fig. 11) are almost certainly attributable to preferred-orientation effects. Observed and calculated d spacings for P3 are given in Table I.

Examination of d spacings previously published for the InSb II phase (supposed tetragonal) show that a much better fit is obtained with the P3 unit cell. One example is set out in Table II, where the d spacings published by McWhan and Marezio[8] are reproduced along with our observed P3 values, expressed as $2\theta$ values at a common incident wavelength of 0.4446 Å, and calculated $2\theta$

values $(2\theta_c)$ are given for the $\beta$-tin unit cell which those authors adopted. As can be seen by comparing columns 4 and 6 in the table, their d spacings correspond closely to a lower resolution version of our P3 pattern in which the bracketed lines are not resolved—as expected on a laboratory source or after passing rapidly through the transition [see the broadened P3 pattern in Fig. 12(b) discussed below]. This correspondence is illustrated in Fig. 5 for the higher-angle part of the pattern: the bars between the P2 and P3 patterns in Fig. 5 show the position of the lines found by McWhan and Marezio[8] in terms of $2\theta$ (Table II), and they all correspond to single lines or to
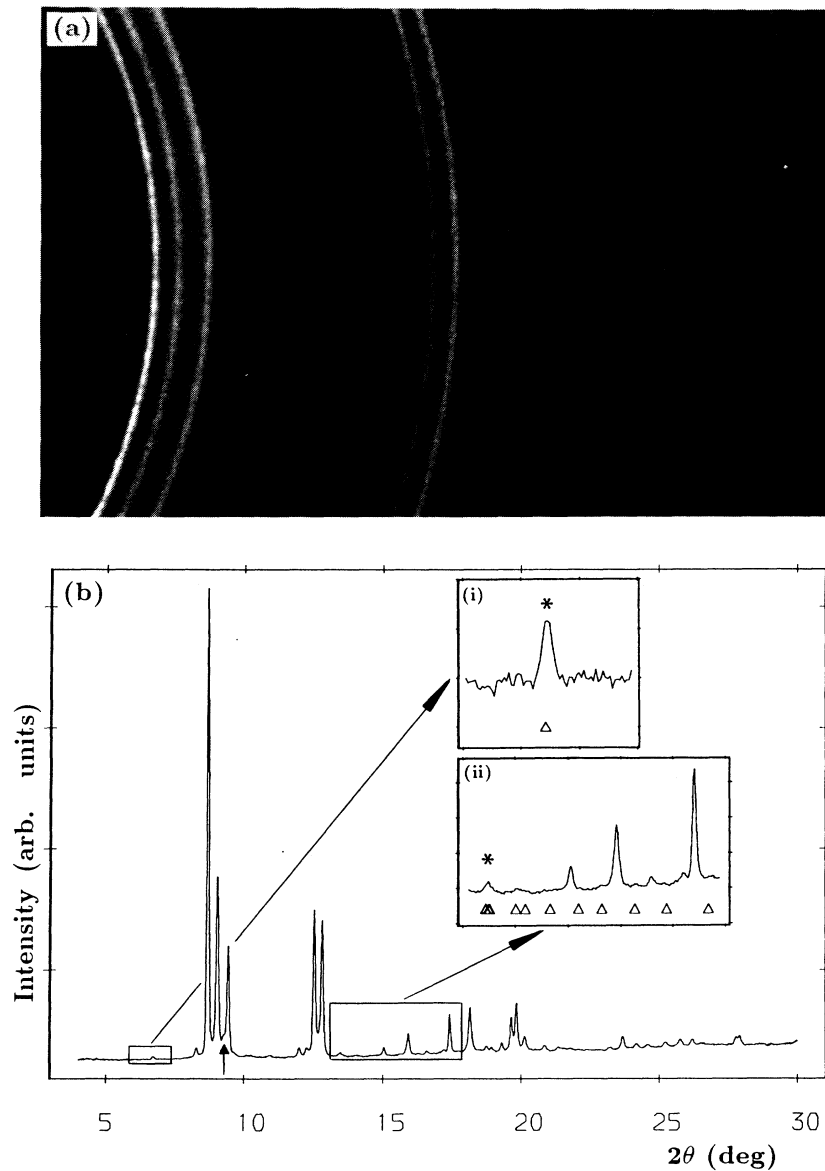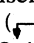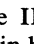


FIG. 8. (a) A pattern recorded from InSb P4 at $\sim$3 GPa, just above the transition directly from the cubic phase. $\lambda = 0.4446$ Å. Exposure time = 42 min. Sample-to-plate distance = 250 mm. (b) The corresponding integrated profile. The insets show parts of the profile enlarged, as indicated. The arrow below the main profile indicates a weak non-P4 line. The marked features in the insets are discussed in the text.

the discrete groups of lines bracketed in Table II. The arrows ($\longrightarrow$ and $\longrightarrow$) show the main discrepancies of the $\beta$-tin indexing (underlined in columns 6 and 7 of Table II), which is evidently unsatisfactory. (It can be seen in both Table II and Fig. 5 that the lines of McWhan and Marezio[8] are all slightly higher in $2\theta$ than our mean $2\theta_0$ values. The average mismatch is equivalent to about 0.4% in the $d$ spacings, which accords closely with the 1.2% volume compression[18] between the pressures of our and their measurements.) Similar results can be obtained for the InSb-II patterns published by Banus et al.[5] and by Banus and Lavine.[9] The reinterpretation of the InSb-

II patterns as $P3$ thus removes the discrepancies summarized in the Introduction—that is, the apparent absence of the $\beta$-tin (220) reflection and the mis-fits shown in Fig. 5. Table II also gives the best-fitting orthorhombic cell dimensions for the InSb-II pattern of McWhan and Marezio,[8] and the results are very similar to those we obtain for $P3$. [The refined volume of 99.6(6) $\text{Å}^3$ at 4.0 GPa corresponds to a value of 100.8(6) $\text{Å}^3$ at the 2.3 GPa of our measurements, as discussed above.]

A further connection with previous work is provided by an experiment in which we intentionally passed rapidly through the transition as McWhan and Marezio[8] did
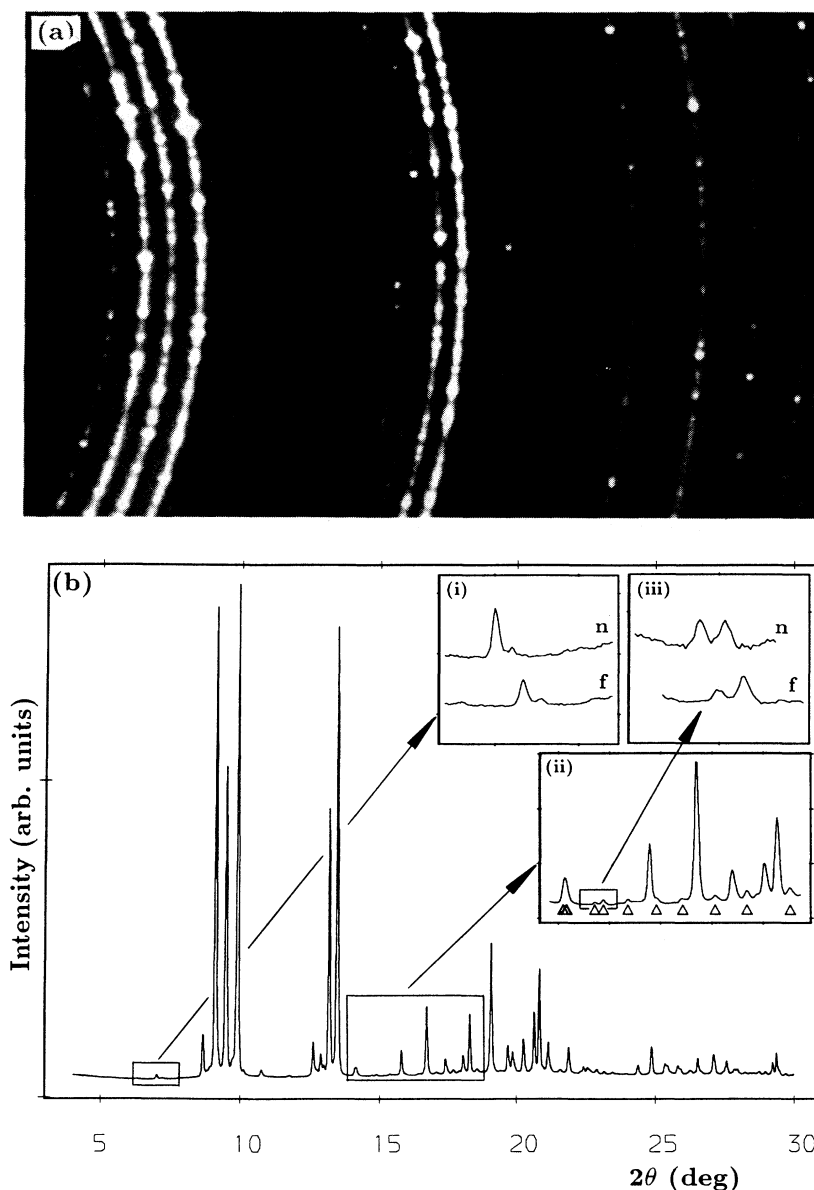


FIG. 9. (a) A pattern recorded from InSb $P4$ at $\sim 2.5$ GPa and 100 °C. $\lambda = 0.4642$ Å. Exposure time $= 146$ min. Sample-to-plate distance $= 250$ mm. (b) The corresponding integrated profile. Inset (i) shows a weak low-angle line recorded with an incident x-ray energy of 26.709 keV, far ($f$) from the In $K$ edge (as in the main profile), and at 27.886 keV, near ($n$) the In $K$ edge (at 27.925 keV). The enlargement in inset (ii) reveals many weak superlattice reflections, marked $\Delta$. Two of these are enlarged further in inset (iii), recorded far from and near the In $K$ edge as in (i).
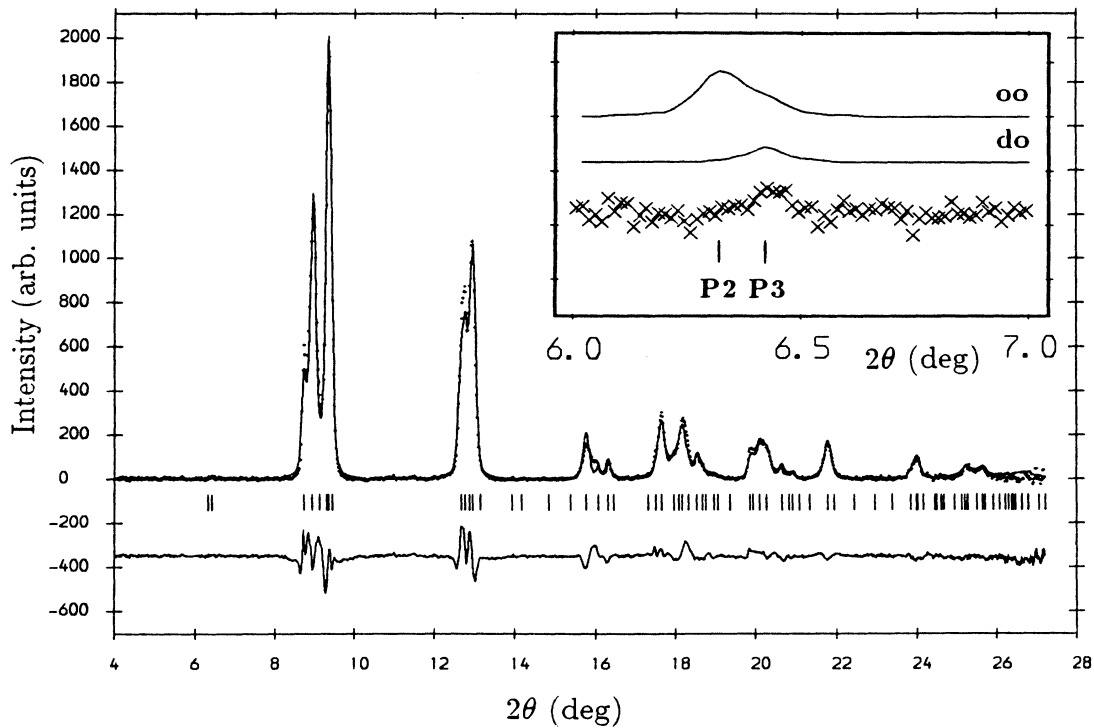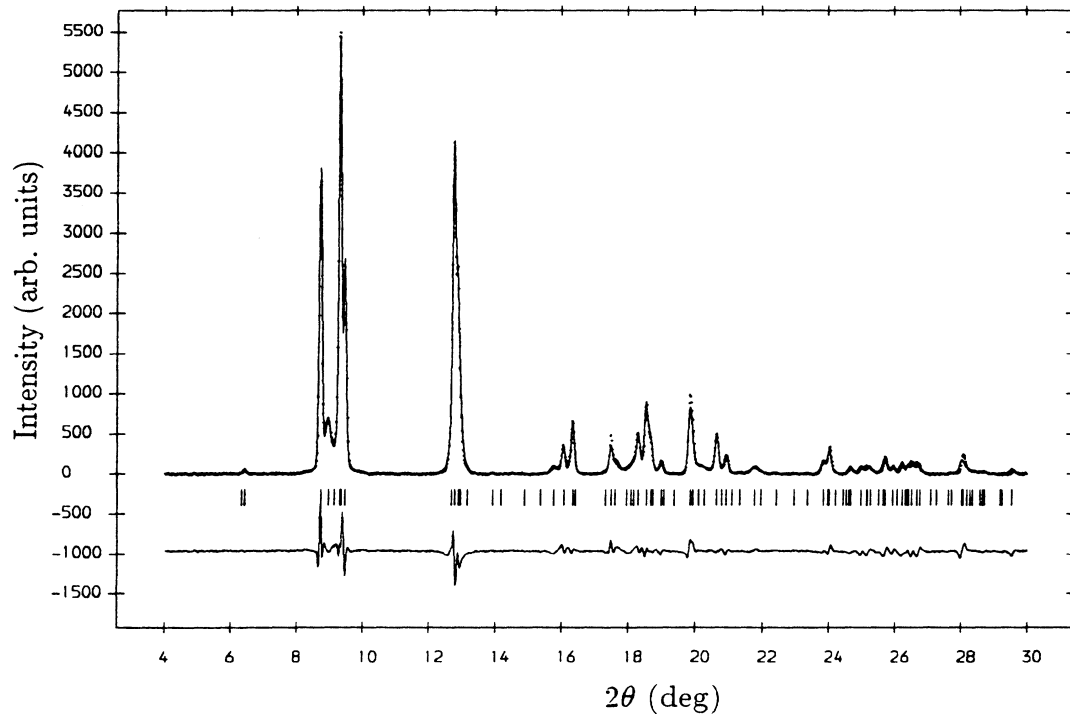
FIG. 10. The fit to the mixed P2-P3 profile in Fig. 3(b) with a multiphase Rietveld refinement. The tick marks show the positions of all reflections allowed by the symmetry. The difference between the observed and calculated profiles is shown below the tick marks. The inset shows the observed profile (crosses) in the vicinity of the lowest-angle reflections of P2 and P3, at the positions marked. Above this are the profiles calculated from the refined fit, with P2 site disordered and P3 site ordered (labeled "do"), and with P2 and P3 both ordered ("oo").



FIG. 11. The fit to the mixed P3-P2 profile in Fig. 4(b) with a multiphase Rietveld refinement. The tick marks show the positions of all reflections allowed by the symmetry. The difference between the observed and calculated profiles is shown below the tick marks.

to obtain the InSb-II phase. This resulted in the rather broadened pattern in Fig. 12(a) which, as shown in Fig. 12(b), slowly and continuously sharpened to the $P3$ pattern of Fig. 4 over a period of 2 days. Even in the initial broadened form the dominant phase is clearly not $\beta$-tin, the principal lines of which are marked by triangles under the profile in Fig. 12(b). One peak of the second doublet is missing (as Kasper and Brandhorst[7] noticed)— compare the $\beta$-tin pattern of the dominant phase in Fig.

3(b)—and there are several other obvious discrepancies which correspond to the $d$ spacing mismatches already rehearsed. However, the shoulder and peak marked by the solid triangles under the initial pattern shows the presence of a weak $P2$ component [compare Fig. 4(b)]. This can be seen to reduce with time and the final pattern has significantly less $P2$ than remains after a more gradual transformation, such as in Fig. 4(b). The inset shows that the weak low-angle line of $P3$ can be seen even in the
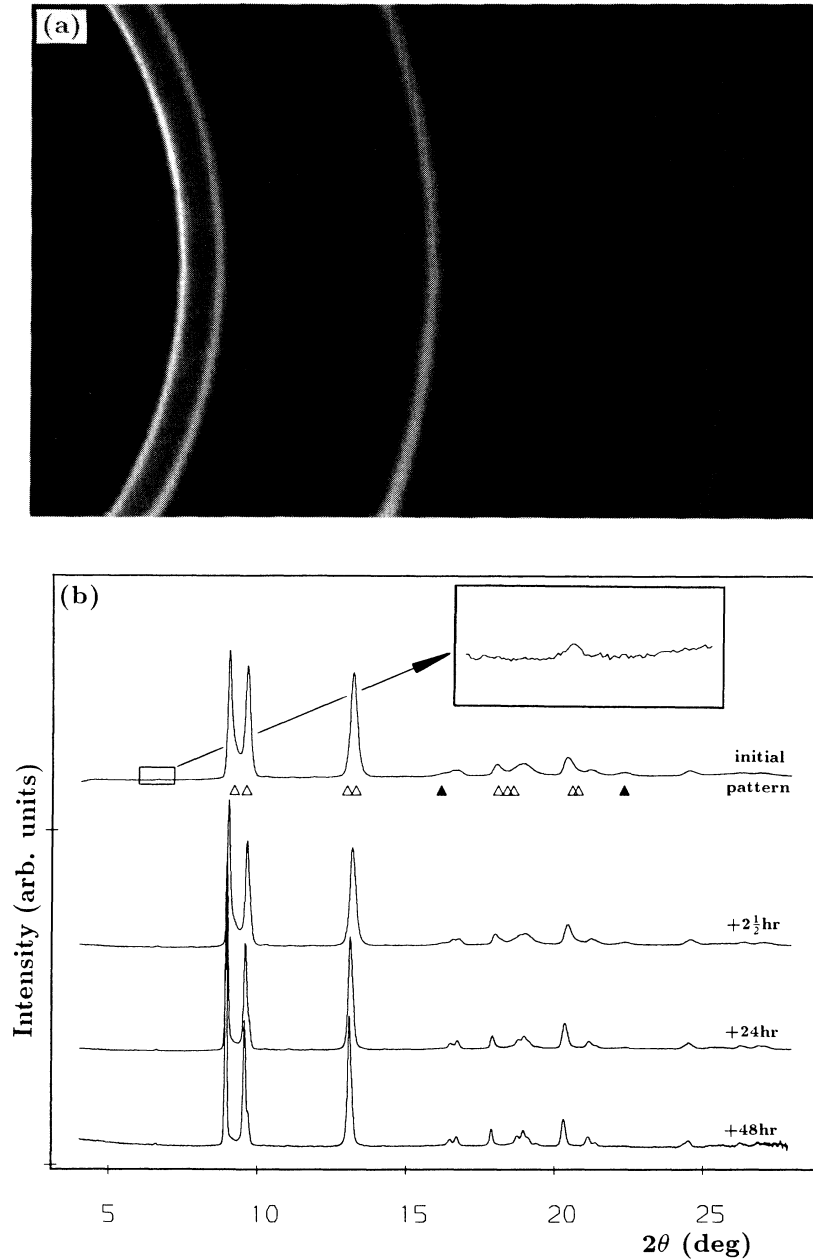


FIG. 12. (a) A pattern recorded from InSb at about 2.3 GPa after passing rapidly through the transition. $\lambda = 0.4442$ Å. Exposure time $= 51$ min. Sample-to-plate distance $= 200$ mm. (b) The corresponding integrated profile, and its subsequent evolution over a period of 2 days. The triangles under the initial profile show the positions of the principal $\beta$-tin lines. The one marked by a solid triangle at $2\theta \sim 22°$ is the nonoverlapping $P2$ line indicated at the same position in Fig. 4(b). The weak low-angle line is enlarged in the inset.

initial pattern, so the broadening is not associated with any disordering of the structure.

One result of fitting the previously published $d$ spacings to an orthorhombic rather than tetragonal cell is that the orthorhombic unit-cell volume is 2–4 % smaller (see Table II). This removes most of the small difference in density previously thought to exist between phases II and IV. Also, the greater density of the orthorhombic description means that the volume collapse at the transition is $\sim 21\%$ rather than $\sim 18.5\%$,[3] in closer agreement with the original direct measurements by Jayaraman et al.[2] The relative unit-cell volumes for $P2$ and $P3$ phases can be obtained from refinements of patterns in which the phases coexist as 100.72(4) $\text{Å}^3$ for $P2$ and 100.21(4) $\text{Å}^3$ for $P3$, so $P3$ is 0.5% denser than $P2$.

### Orthorhombic phase P4

All the readily visible peaks of the $P4$ pattern can be indexed on an orthorhombic unit cell with $a = 2.925(1)$ Å, $b = 5.617(1)$ Å, and $c = 3.067(1)$ Å. This is the same as InSb IV, and Fig. 13 shows that the intensities are well fitted by the structure proposed by Yu et al.[16] (space group $Pmm2$) with atoms at (0,0,0) and $(0,\frac{1}{2},\alpha)$. Our refined value of $\alpha = 0.387(1)$ is in close agreement with Vanderborgh et al.[18] We discuss the ordering of the structure below.

The observed profile used for the structure refinement is the one obtained by recrystallization from the $P3$ phase at 100 °C [Fig. 9(b)], as this gave single-phase $P4$. [This

profile is identical with the $P4$ component of the $P3$-$P4$ mixture at room temperature shown in inset (ii) of Fig. 6(b).] By contrast with the good fit obtained to the pattern of $P4$ recrystallized from $P3$ (Fig. 13), it is impossible to fit the $Pmm2$ structure to the pattern obtained by direct transformation from the cubic phase [Fig. 8(b)] without large intensity differences. These are systematic with $(hkl)$, being greatest for reflections with $l > h, k$, and we conclude that the pattern in Fig. 8(b) is affected by preferred orientation.

Although it is clear that $P4$ is the InSb-IV phase, the true structure is much more complex than supposed. Inset (ii) in Fig. 9(b) shows many weak lines (marked $\triangle$) not accounted for by the $a \times b \times c$ $Pmm2$ unit cell. All these superlattice reflections can be indexed on a $2a \times 3b \times 2c$ unit cell, with absences corresponding to $B$-face centering. [The insets in Fig. 8(b) show that the superlattice reflections are also present in the case of the direct transition, though only the strongest ones (marked *) stand out clearly. The reflection in inset (i) of Fig. 8(b) is a sufficient signature of the $2a \times 3b \times 2c$ cell since it indexes as (121) on that cell.] Inset (iii) in Fig. 9(b) shows a pair of superlattice reflections, further enlarged, recorded far $(f)$ from the In $K$-absorption edge and near $(n)$ it—as for $P3$ in Fig. 4(b). Inset (i) in Fig. 9(b) shows the same for a low-angle reflection. The clear increases in relative intensity near the In edge shows that at least part of the intensity in these lines arises from the difference in scattering between In and Sb: hence the structure is site ordered.

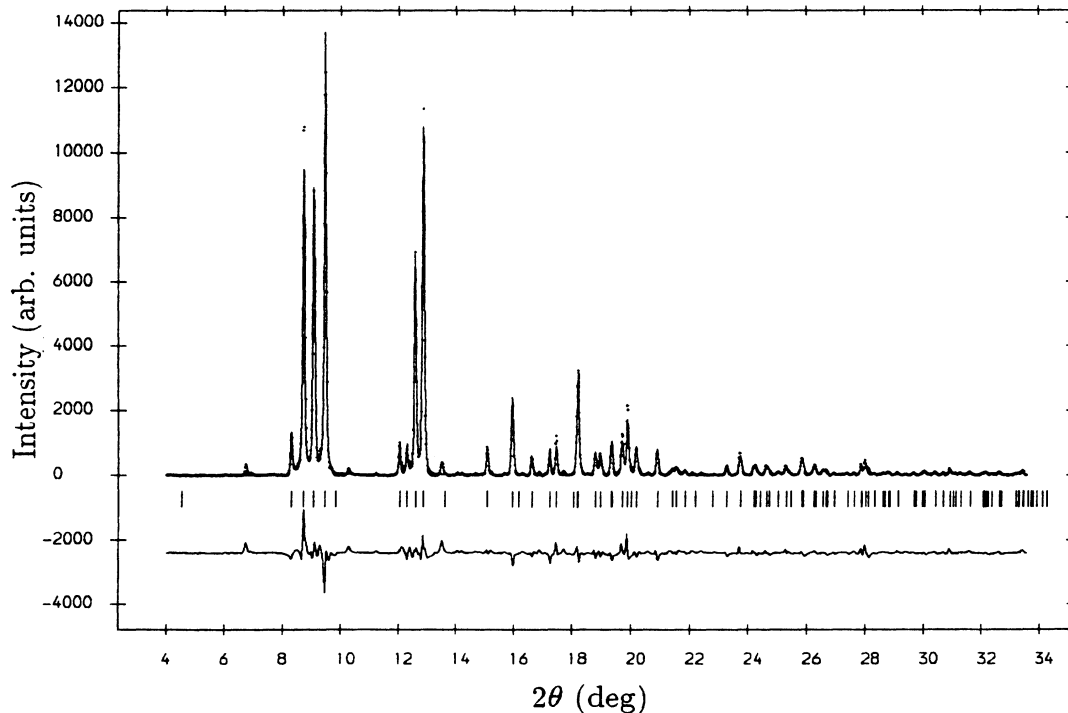The previously proposed $Pmm2$ structure of InSb IV



FIG. 13. The fit to the $P4$ profile in Fig. 9(b). The tick marks show the positions of all the reflections allowed by the $Pmm2$ average structure. The difference between the observed and calculated profiles is shown below the tick marks.

thus emerges as an average subcell of the true, much larger unit cell. Work is currently in progress to try to determine the complete structure. The distortions required to produce such weak superlattice reflections are very small, and have a negligible effect on the subcell pattern. (Hence the introduction of the true cell does not invalidate the preceding remarks about preferred orientation.) Table I gives the observed and calculated $d$ spacings for the subcell reflections only—indexed both on the true cell, $hkl$, and on the subcell, $hkl_s$. The volume per atom in the subcell (the $V/N_A$ in Table I) can be seen to be very close to that of the $P3$ phase. Refinements of mixed-phase patterns show that $P4$ is 0.5% *less* dense.

## IV. DISCUSSION AND CONCLUSIONS

The results we have obtained remove a number of previous problems and uncertainties, but also raise several new questions about the phase transitions and $P$-$T$ phase diagram of InSb. In the following discussion we attempt to draw together the threads of our own and previous work, and summarize what we believe to be now established.

Figures 2 and 3 show $P2$ always accompanied by the same amount of $P3$ (about 30% in this case) from the first emergence of the high-pressure phases as cubic InSb transforms to $P2$ and $P3$. This could be interpreted in two ways. If the transformation is from cubic to $P2$ and then to $P3$, the pressure range of stability must be less than the variation in pressure across the sample, so that the two transformations overlap; or it could be that the cubic phase transforms directly to $P3$, some of which then transforms to $P2$ with the *decrease* in pressure accompanying the volume collapse of the cubic to $P3$ transition. (Vanderborgh et al.[18] measured a 0.2-GPa drop in pressure for the cubic to $P4$ transition, which has almost the same magnitude of volume collapse.) Refinements of two-phase $P2$-$P3$ patterns all show that $P3$ is the slightly more dense, by about 0.5%. This very small difference in density between $P2$ and $P3$ probably accounts for the persistence of a few percent of $P2$ to much higher pressures. We cannot obtain a reliable estimate of the cubic phase to $P2$-$P3$ volume collapse from mixed patterns because, as previously remarked, the cubic phase either completely dominates (Fig. 2) or is almost absent [Fig. 3(b)]. Taking earlier work and reindexing InSb II as $P3$ (see Sec. III) gives an estimate of $\sim$21% for the volume change from cubic to $P3$.

There are several distinct differences between $P2$ and $P3$: the peaks of $P2$ are significantly broader [Figs. 3(b) and 4(b)], $P3$ is site ordered while $P2$ appears not to be long-range ordered (i.e., there is no measurable In-Sb difference peak), and the $P2$ pattern seems to be less affected by preferred orientation. It is intriguing that two phases with such similar densities and crystal structures should differ so much in these other ways. The broadening of the $P2$ peaks does not show a strong $2\theta$ dependence [see Fig. 3(b)] and so is probably due to small crystallite size rather than strain. Then it is interesting to note that both steps in the sequence $P2 \rightarrow P3 \rightarrow P4$ are characterized by a significant increase in crystallite size.

The excess broadening of the $P2$ lines in Fig. 3(b) indicates a particle size of the order of a few tens of nanometers in that phase. Then the density of $P4$ spots in Fig. 6(a), and their peak intensity compared with that of the (smooth) $P3$ lines, suggest a particle size of a few hundreds of nanometers in $P3$ and over a micron in $P4$.

The evidence that $P2$ is not long-range site ordered raises interesting questions about the role of such a structure as an intermediate stage in the transition from ordered cubic InSb to ordered $P3$. As discussed briefly by Vanderborgh et al.,[18] it seems that energy considerations must favor a structure in which each atom is surrounded by six unlike nearest neighbors, and hence is site ordered, as in $P3$. Of course, the fact that the In-Sb difference peaks cannot be detected does not necessarily imply entirely random site occupancy. It is physically more reasonable to envisage some degree of short-range ordering, characterized by a correlation length. All that can be said from the diffraction results is that this length must be somewhat smaller than the particle size.

The recrystallization of $P3$ to $P4$ appears to take place most readily at a pressure just above the cubic to $P3$ transition, so the stability field of $P3$ is evidently very narrow. Indeed we have some evidence of $P3$ starting to change to $P4$ even before all of the cubic phase has transformed, so there may be no stability field for $P3$ at room temperature. Refinements of two-phase $P3$-$P4$ patterns show that $P4$ is slightly *less* dense than $P3$, by about 0.5%. However, this comparison is made for the crystalline grains contributing to the sharp diffraction lines: the large $P4$ grains [giving the spots in Fig. 6(a)] are embedded in a mixture of relatively small $P3$ grains *and* intergrain $P3$ material, so that the overall density of this mixture may be less than that of $P4$. In any case, the difference in density is very small and this probably accounts for the fact that the $P3$ to $P4$ transformation is sluggish, not proceeding beyond approximately 50:50 proportions (at room temperature) and strongly inhibited by higher pressures (the in-grain density difference remains about the same as pressure is increased).

The evident spottiness of patterns such as the one shown in Fig. 6(a) raises the question as to why this behavior has not been reported before. The 2D image at $\sim$2.5 GPa published by Hanneman et al.[6] is heavily contaminated by Laue spots from the diamond anvils, which might obscure (or be taken to be the reason for) similar features from the sample. This will also apply to the work of Smith and Martin,[3] Banus et al.[5] (the same pattern as the one published by Hanneman et al.[6]), and Banus and Lavine.[9] McWhan and Marezio[8] used a monochromator, which would reduce the problem of Laue spots from the anvils, but the sample was taken quickly to a pressure (4.0 GPa) which inhibits the transformation to $P4$. Kasper and Brandhorst[7] also appear to have recorded their patterns at pressures above 3.0 GPa. (In fact, the 2D pattern published by Hanneman et al.[6] appears to be labeled "32 kilobars." If this is correct, their pattern joins those recorded above the pressure range where $P3$ transforms readily to $P4$.) In addition, there is the consideration, applying to all this earlier work, that the lower angular resolution of laboratory-

source techniques would greatly reduce the height, and hence visibility, of individual diffraction spots above background. As discussed below, the one previous (but energy-dispersive) synchrotron study[18] may have observed P4 recrystallized from P3, but spottiness in the pattern would not be directly detected in an energy-dispersive measurement.

Questions about what has been seen before also attach to the mixed P3-P4 patterns we have frequently obtained [as in Fig. 6(b)]. The arguments above apply again, in that all but one[9] of the reported studies of P3 appear to have been at pressures high enough to inhibit the appearance of P4. Also, the lower resolution of patterns collected on laboratory sources would make the difference between P3 [Fig. 4(b)] and the mixed pattern [Fig. 6(b)] difficult to detect—apart perhaps from the P4 peak in the middle of the group near $2\theta=9°$ [Fig. 6(b)], but this would be rather weak unless the transformation had proceeded to something approaching 50% of P4. However, the one previous synchrotron study[18] does report a pattern interpretable as a P3-P4 mixture. Figure 14 shows our mixed P3-P4 pattern from Fig. 6(b) with the five main, nonoverlapping P3 peaks filled in and indexed [these are the reflections marked * in Fig. 6(b)]. Vanderborgh et al.[18] focus attention on the triplet they find at the position marked T (Fig. 14) in an energy-dispersive pattern collected at 6.3 GPa, remarking that the central peak is a new line which cannot be indexed. Although they do not note the fact explicitly, their pattern also has three unexplained doublets formed by additional reflections at the positions marked D in Fig. 14. (The second triplet T' is hidden by fluorescence lines.) The authors attribute these features to a new phase, InSb V, but it seems more probable that they obtained a mixture of P3 and P4. Their pattern corresponds closely to ours (Fig. 14), but with a slightly higher proportion of P3. And as best as can be measured from Figs. 1 and 2 of their paper, the relative densities of the two phases agree with our observations: we obtain cell dimensions $a = 2.897(3)$ Å, $b = 5.557(3)$ Å, $c = 3.038(6)$ Å for their P4, and $a = 5.76(6)$ Å, $b = 5.32(2)$ Å, $c = 3.17(1)$ Å from the four visible nonoverlapping peaks of their P3 (indexed as in Fig. 14), giving a density for P3 $0.7\pm1.0\%$ greater than that of P4. (These P3-P4 unit-cell volumes are ~3% less than in our measurements because Vanderborgh et al.[18] were working at a higher pressure of 6.3 GPa. We have adjusted for this difference in deriving the relative positions shown in Fig. 14.) There is one further unexplained peak in the energy-dispersive pattern, at the position marked S in Fig. 14. This cannot be indexed as a P3 or P4 subcell line, but can be seen to align with a peak in our pattern which is from the residual component of P2.

It seems, then, that Vanderborgh et al.[18] have observed the same three-phase mix of P2, P3, and P4 as we report. However, they appear to say that this pattern developed from a pure P4 pattern, which is a sequence we have never seen. It would be interesting to know whether this really is an example of P4 transforming to P2-P3, or is in fact a different loading in which the cubic phase first transformed to P2-P3 and then to P4 as we
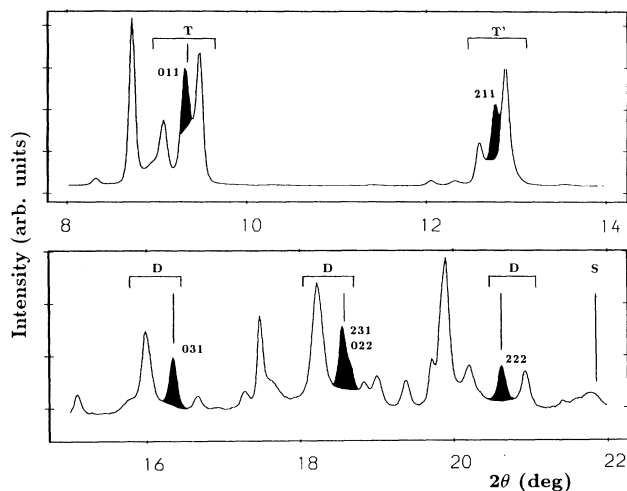


FIG. 14. The mixed P3-P4 pattern of Fig. 6(b) with the nonoverlapped P3 peaks filled in and indexed. The vertical lines show the positions of additional peaks observed in a P4 pattern recorded by Vanderborgh et al. (Ref. 18) at 6.3 GPa, adjusted to a common unit-cell volume to allow for the difference in sample pressure. These give rise to the triplet (T) discussed by Vanderborgh et al. (Ref. 18), to three doublets (D) and a singlet (S). The second triplet (T') is obscured by fluorescence peaks in the energy-dispersive study (Ref. 18).

have always observed.

If pressure is increased gradually on polycrystalline cubic InSb, it seems that the transition to P3 does not occur and the sample becomes superpressed, with a direct transition to P4 then taking place at a pressure well above that at which P4 recrystallizes from P3. Reported values for the required pressure vary more than for the cubic to P3 transition—about 3.0 GPa in Kasper and Brandhorst,[7] $2.5\pm0.2$ GPa in Yu et al.,[16] 3.05 GPa in Turusbekov and Estrin,[30] 2.8 GPa in Vanderborgh et al.,[18] and around 3.0 GPa in our work. In the case of single-crystal samples, all the reported transition pressures are close to 3.0 GPa,[1,31–33] with one exception[6] where the transition occurred at ~2.3 GPa. Diffraction patterns of the high-pressure phase were not obtained in any of these single-crystal experiments, but it seems very probable that the transitions reported at 3.0 GPa are to P4. If so, it is worth noting that the very first report of the high-pressure transition in InSb by Gebbie et al.[1] (at ~3 GPa) was therefore to P4 rather than P3, four years before P4 was identified by Kasper and Brandhorst.[7]

There are some interesting differences to be seen in the powder patterns between the cubic to P2-P3 and cubic to P4 transitions. Comparison of Figs. 2 and 7 shows that the cubic phase is significantly more broadened at the start of the direct cubic to P4 transition, and this is a reproducible effect. Comparison of insets (i) and (iii) of Fig. 7 with inset (ii) of Fig. 6(b) reveals (as already remarked) that the middle one of the first triplet of P4 lines is offset toward lower $2\theta$ in the cubic-P4 pattern (Fig. 7). This shows that the shape of the orthorhombic unit cell for P4 transforming from the cubic phase is a lit-

tle different from what it is for $P4$ growing from $P3$, though the volume collapse is the same (19.5%) in both cases. Also, the shape of the unit cell becomes the same in both cases once the transition from cubic to $P4$ is complete [compare Figs. 8(b) and 9(b)]. These features may be relevant to whatever determines the route to $P4$ from the cubic phase (via $P3$ or direct) and the difference in transition pressures.

The volume collapse of 19.5% which we obtain from cubic-$P4$ mixed patterns is significantly greater than the 17.1% derived by Vanderborgh et al.,[18] also from a mixed pattern. We have no explanation for this. Measurements of $V/V_0$ in the cubic and high-pressure phases[13,18] show that the cubic phase is approximately three times more compressible in the 2–3 GPa range, in which case the volume collapse for the cubic to $P3$ transition at $\sim 2.1$ GPa should be $\sim 1\%$ greater than for cubic to $P4$ at $\sim 3.0$ GPa. This accords with our estimates of

$\sim 21\%$ and 19.5%, respectively, and the latter value agrees with the 19.3(1)% measured by Yu et al.[16,34] The results of Vanderborgh et al.[18] would give a change of only 18% for the cubic to $P3$ transformation.

Broadly speaking it is evident that fast pressure increase under strained or nonhydrostatic conditions favors the transition from cubic to $P2$-$P3$, while increasing the pressure slowly under more uniform conditions favors the transition from cubic to $P4$. At one extreme is the strained $P3$ produced by McWhan and Marezio[8] and by us (Fig. 12), through an intentionally over-rapid pressure increase. At the other extreme is a single crystal under pure hydrostatic conditions where a transition pressure as high as 3.15 GPa has been reported by Okai and Yoshimoto.[31] These authors showed that under conditions of uniaxial stress the transition could be observed occurring from 2.2 GPa down to as low as 1.8 GPa, and it would be interesting to know if the high-pressure phase
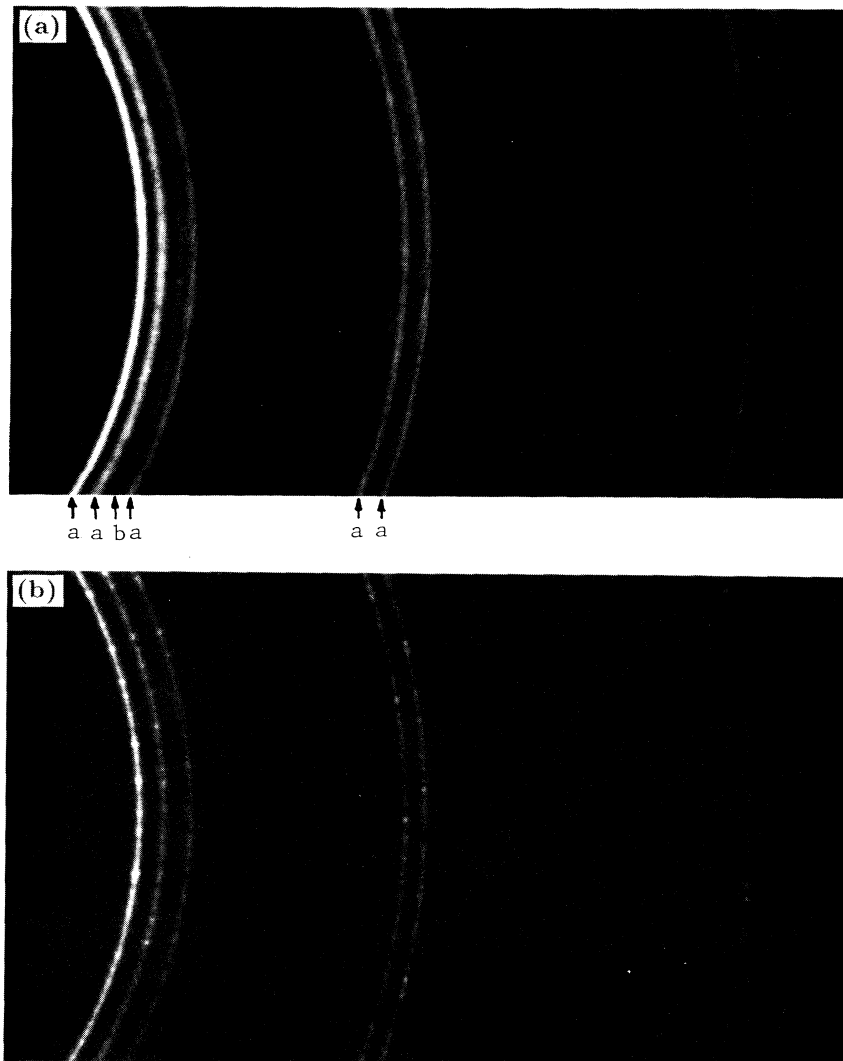


FIG. 15. (a) A mixed $P3$-$P4$ pattern recorded from InSb after passing through the transition at $\sim 3.0$ GPa. The strongest $P4$ lines are labeled "a," and the single visible $P3$ line is labeled "b." $\lambda = 0.4446$ Å. Exposure time $= 26$ min. Sample-to-plate distance $= 250$ mm. (b) A pattern recorded from the same sample 15 h later, after $P3$ has recrystallized to $P4$. $\lambda = 0.4446$ Å. Exposure time $= 42$ min. Sample-to-plate distance $= 250$ mm.

is then P3. Away from the extremes it is far less clear what are the crucial factors. Certainly we find no difference at all between samples of 99.99% and 99.9999% purity. In some as yet limited tests of the influence of hydrostaticity we have found no clear difference in behavior between dry samples (no methanol:ethanol) and samples loaded with a greater than normal amount of methanol:ethanol. An indication of the fine balance between the two routes from cubic InSb to P4 is afforded by the sequence shown in Fig. 15 for a sample loaded with the "normal" amount of methanol:ethanol. At the stage shown in Fig. 15(a), most of the sample has transformed directly to P4, giving the characteristic smooth P4 lines (e.g. as labeled "a"), and the remaining small amount of cubic phase has then followed the other route and transformed to P2-P3 as shown by the line labeled "b"; at the later stage shown in Fig. 15(b), this last line, "b," has vanished as P3 recrystallizes to P4, and spots have appeared on the hitherto smooth P4 lines. Without any known changes of external conditions, both routes have been followed in the same sample. [The fact that some of the sample may transform to P2-P3 when most of it is transforming to P4 would account for the weak residual feature marked in Fig. 8(b).]

Although there are thus many details of the high-pressure behavior of InSb yet to be understood, it is clear that the P-T phase diagram needs to be revised. If there is any pressure range in which P3 is the equilibrium phase at room temperature, our results indicate it to be no more than about 0.1 GPa wide. Above that range, P4 is the equilibrium phase. In addition, there may be an equally narrow field (if any at all) between the cubic phase and P3 in which P2 is the equilibrium phase; alternatively P2 may be metastable or appear only on pressure decrease. In one experiment carried out by heating to 50 °C in the cubic phase and then applying pressure, the product was a mixture of P2 and P3. As discussed in Sec. III, the same procedure at 100 °C gave a clean P4 pattern which we interpreted as having been reached via P3. This evidence indicates a boundary between P3 and P4 at approximately constant pressure, and we do not then expect the transition from P4 to P3 (InSb IV to InSb II) on heating shown in the phase diagram of Banus and Lavine.[9] So far we have been able to make only a few direct tests of this. A mixed sample of P2 and P3 heated to 60 °C transformed to P3, and after further time at the same temperature made an accelerated transition to P4. Another sample starting as a mixture of P3 and P4 at a higher pressure was converted to P4, but with some P3 remaining, after 10 h at 75–100 °C. These results support the conclusion that the equilibrium field of P4 extends well above room temperature at pressures up to ~3.0 GPa, contrary to the accepted phase diagram.

Banus and Lavine's derivation of their phase diagram[9,11] was based strongly on identifying InSb II with the β-tin phase obtained on cooling to 77 K and then down-loading to ambient pressure. This was clearly incorrect. The belief that InSb II was the equilibrium phase above room temperature and the subsequent discovery of InSb IV at room temperature led to some prejudgment of the boundary between InSb II and InSb

IV. Between the first transition (2.3 GPa) and 3.7 GPa no measurements are shown to support the proposed II-IV boundary,[9] and where there are measurements it can be seen how they might have been interpreted differently without the prior expectations. However, there is at least one reported experiment that cannot be explained this way: the authors[9] appear to say that they monitored an InSb-IV (P4) pattern transforming to InSb-II (P3) at 85 °C and 4.5 GPa. The only other report we can find of a direct investigation of heating P4 is in the work of Yu et al.[16] They heated InSb-IV (P4) to 100 °C at 4.6 GPa (almost the same pressure as in Banus and Lavine's experiment[9] above), and obtained "a different x-ray pattern" which they could not interpret. (This suggests it was not InSb II.) Since all previous high-temperature diffraction work has been above 3.7 GPa, with corroboration only at ~4.5 GPa, and our heating experiments have been at ~3.0 GPa and below, a possible interpretation is that, although P4 is the equilibrium phase to 100 °C or higher in the range up to ~3.0 GPa, there is a transition to another phase not far above room temperature at higher pressures.

In summary, our main conclusions are as follows.

1. The reproducible behavior of cubic InSb at room temperature is either to transform at ~2.1 GPa to a mixture of P2 and P3, which then transforms to nearly single-phase P3 before recrystallizing to P4 at the same or only slightly higher pressures, or else to transform directly to P4 at ~3.0 GPa.

2. P2 is a tetragonal phase with a β-tin structure. This is not InSb II, but may be the phase previously seen on recovery to ambient pressure at low temperature. The structure appears not to be long-range site ordered in that In-Sb difference peaks cannot be detected.

3. P3 is the InSb-II phase, which is shown to have an orthorhombic structure rather than β-tin as previously supposed. This structure is site ordered.

4. P4 is the (orthorhombic) InSb-IV phase, but this is now shown to have superlattice reflections that can be indexed on a unit cell 12 times larger than the Pmm2 cell of Yu et al.[16] This structure is also site ordered.

5. It seems possible to account for all previous (clear) results on InSb at room temperature with these three phases and mixtures of them. In particular, a P2-P3-P4 mixture accounts for the pattern recently attributed by Vanderborgh et al.[18] to a new phase (InSb V).

6. The accepted P-T phase diagram of InSb is incorrect, and needs to be revised. In particular, there does not seem to be a transition from P4 (InSb IV) to P3 (InSb II) on heating to at least 100 °C in the range up to ~3.0 GPa. Substantial further work is needed to clarify the regions of stability of the known phases. While the phase diagram remains so uncertain, it is proposed to adopt the simple labeling scheme P1, P2, . . ., for phases as they are found.

The two different paths from the cubic phase to P4, the existence in a very small pressure range of three quite different high-pressure phases with similar structural coordination and densities differing by only ~0.5%, and other observations such as the transition from amorphous InSb to an NaCl structure in the same pressure range,[35,36]

all show InSb to be a very finely balanced system. It remains to be seen whether it is exceptional in the complexity of behavior now revealed.

Finally, we remark that the results presented in this paper illustrate the large gain in sensitivity achievable using angle-dispersive techniques with the image-plate area detector and pattern integration—provided care is taken to minimize nonsample scattering and background levels. We have been almost overwhelmed by new information in what was originally expected to be a relatively simple experiment.

## ACKNOWLEDGMENTS

[1] H. A. Gebbie, P. L. Smith, I. G. Austin, and J. H. King, Nature (London) **188**, 1096 (1960).

[2] A. Jayaraman, R. C. Newton, and G. C. Kennedy, Nature (London) **191**, 1288 (1961).

[3] P. L. Smith and J. E. Martin, Nature (London) **196**, 762 (1962).

[4] J. C. Jamieson, Science **139**, 845 (1963).

[5] M. D. Banus, R. E. Hanneman, A. N. Mariano, E. P. Warekois, H. C. Gatos, and J. A. Kafalas, Appl. Phys. Lett. **2**, 35 (1963).

[6] R. E. Hanneman, M. D. Banus, and H. C. Gatos, J. Phys. Chem. Solids **25**, 293 (1964).

[7] J. S. Kasper and H. Brandhorst, J. Chem. Phys. **41**, 3768 (1964).

[8] D. B. McWhan and M. Marezio, J. Chem. Phys. **45**, 2508 (1966).

[9] M. D. Banus and M. C. Lavine, J. Appl. Phys. **40**, 409 (1969).

[10] Y. Kato and T. Ikezu, Phys. Lett. **23**, 644 (1966).

[11] M. D. Banus and M. C. Lavine, J. Appl. Phys. **38**, 2042 (1967).

[12] A. J. Darnell and W. F. Libby, Science **139**, 1301 (1963).

[13] A. J. Darnell and W. F. Libby, Phys. Rev. **135**, A1453 (1964).

[14] S. Geller, D. B. McWhan, and G. W. Hull, Science **140**, 62 (1963).

[15] T. F. Stromberg and C. A. Swenson, Phys. Rev. **134**, A21 (1964).

[16] S. C. Yu, I. L. Spain, and E. F. Skelton, J. Appl. Phys. **49**, 4741 (1978).

[17] V. F. Degtyareva, I. T. Belash, G. V. Chipenko, E. G. Ponyatovskii, and V. I. Rashchupkin, Fiz. Tverd. Tela (Leningrad) **25**, 2968 (1983) [Sov. Phys. Solid State **25**, 1712 (1983)].

[18] C. A. Vanderborgh, Y. K. Vohra, and A. L. Ruoff, Phys. Rev. B **40**, 12 450 (1989).

[19] S. B. Zhang and M. L. Cohen, Phys. Rev. B **35**, 7604 (1987).

[20] R. J. Nelmes, P. D. Hatton, M. I. McMahon, R. O. Piltz, J. Crain, R. J. Cernik, and G. Bushnell-Wye, Rev. Sci. Instrum. **63**, 1039 (1992).

[21] R. O. Piltz, M. I. McMahon, J. Crain, P. D. Hatton, R. J. Nelmes, R. J. Cernik, and G. Bushnell-Wye, Rev. Sci. Instrum. **63**, 700 (1992).

[22] R. J. Nelmes, P. D. Hatton, M. I. McMahon, R. O. Piltz, and J. Crain, in *Proceedings of XIII AIRAPT Conference*, Bangalore, 1991, edited by A. K. Singh (Oxford & IBH, New Delhi, 1992); P. D. Hatton, M. I. McMahon, R. O. Piltz, J. Crain, and R. J. Nelmes, High Pressure Res. **9**, 194 (1992).

[23] R. J. Nelmes, M. I. McMahon, P. D. Hatton, R. O. Piltz, J. Crain, R. J. Cernik, and G. Bushnell-Wye, High Pressure Res. **8**, 677 (1992).

[24] Y. Fujii, K. Hose, Y. Ohishi, H. Fujihisa, N. Hamaya, K. Takemura, O. Shimomura, T. Kikegawa, Y. Amemiya, and T. Matsushita, Phys. Rev. Lett. **63**, 536 (1989); O. Shimomura, K. Takemura, H. Fujihisa, Y. Fujii, Y. Ohishi, T. Kikegawa, Y. Amemiya, and T. Matsushita, Rev. Sci. Instrum. **63**, 967 (1992); T. Kikegawa, High Pressure Res. **8**, 631 (1992).

[25] L. Merrill and W. A. Bassett, Rev. Sci. Instrum. **45**, 290 (1974).

[26] D. M. Adams, Diacell Products, 54 Ash Tree Road, Leicester, UK.

[27] G. J. Piermarini and S. Block, Rev. Sci. Instrum. **46**, 973 (1975).

[28] H. M. Rietveld, J. Appl. Crystallogr. **2**, 65 (1969).

[29] A. N. Fitch and A. D. Murray (unpublished).

[30] T. M. Turusbekov and E. I. Estrin, Fiz. Tverd. Tela (Leningrad) **24**, 286 (1982) [Sov. Phys. Solid State **24**, 163 (1982)].

[31] B. Okai and J. Yoshimoto, J. Phys. Soc. Jpn. **45**, 1880 (1978).

[32] E. G. Ponyatovskii and G. I. Peresada, Dok. Akad. Nauk SSSR **144**, 307 (1962) [Sov. Phys. Dokl. **7**, 408 (1962)].

[33] D. R. Yoder-Short, R. Colella, and B. A. Weinstein, Phys. Rev. Lett. **49**, 1438 (1982).

[34] S. C. Yu, I. L. Spain, and E. F. Skelton, Solid State Commun. **25**, 49 (1978).

[35] K. Asaumi, O. Shimomura, and S. Minomura, J. Phys. Soc. Jpn. **41**, 1630 (1976).

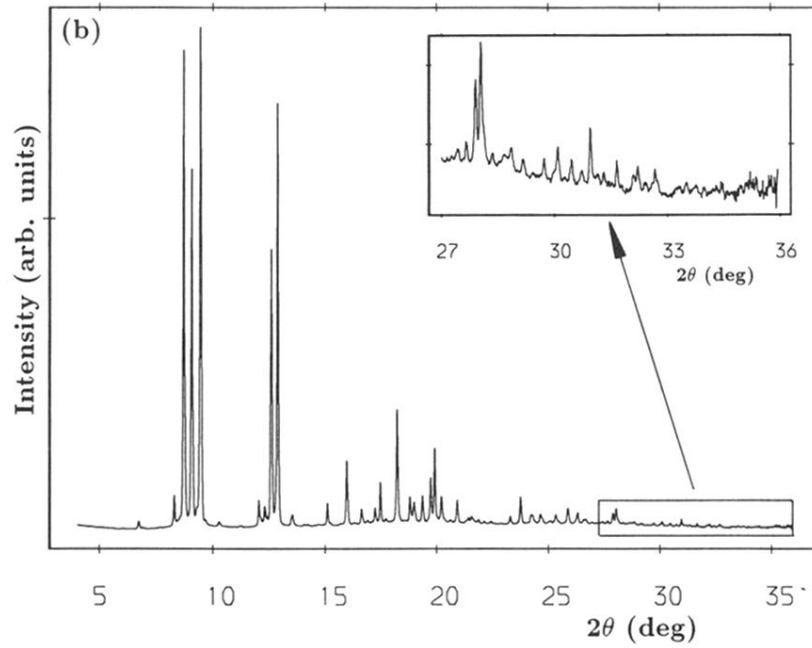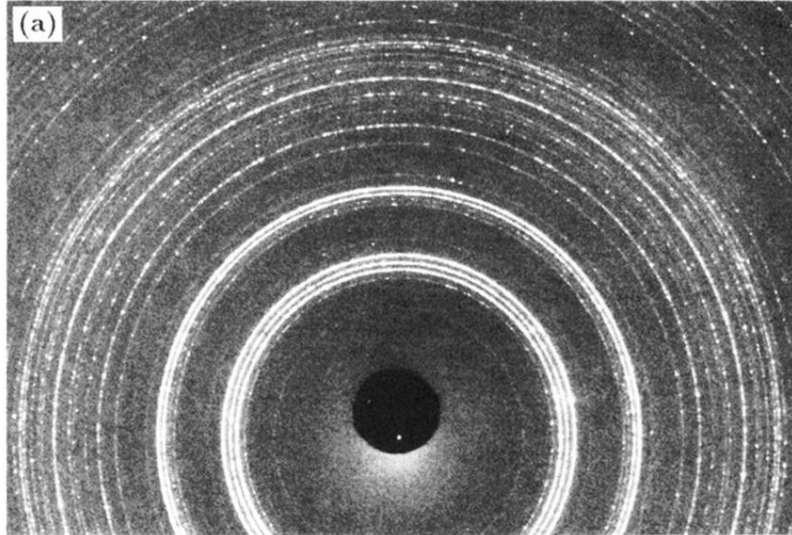[36] O. Shimomura, K. Asaumi, N. Sakai, and S. Minomura, Philos. Mag. **34**, 839 (1976).

FIG. 1. (a) A full two-dimensional powder pattern recorded from InSb at a sample-to-plate distance of 250 mm, using an incident wavelength of 0.4446 Å. The sample was held in a Merrill-Bassett diamond-anvil cell at ~2.5 GPa. Exposure time was 84 min. (b) The corresponding integrated profile. The high-angle part of the profile is enlarged in the inset.

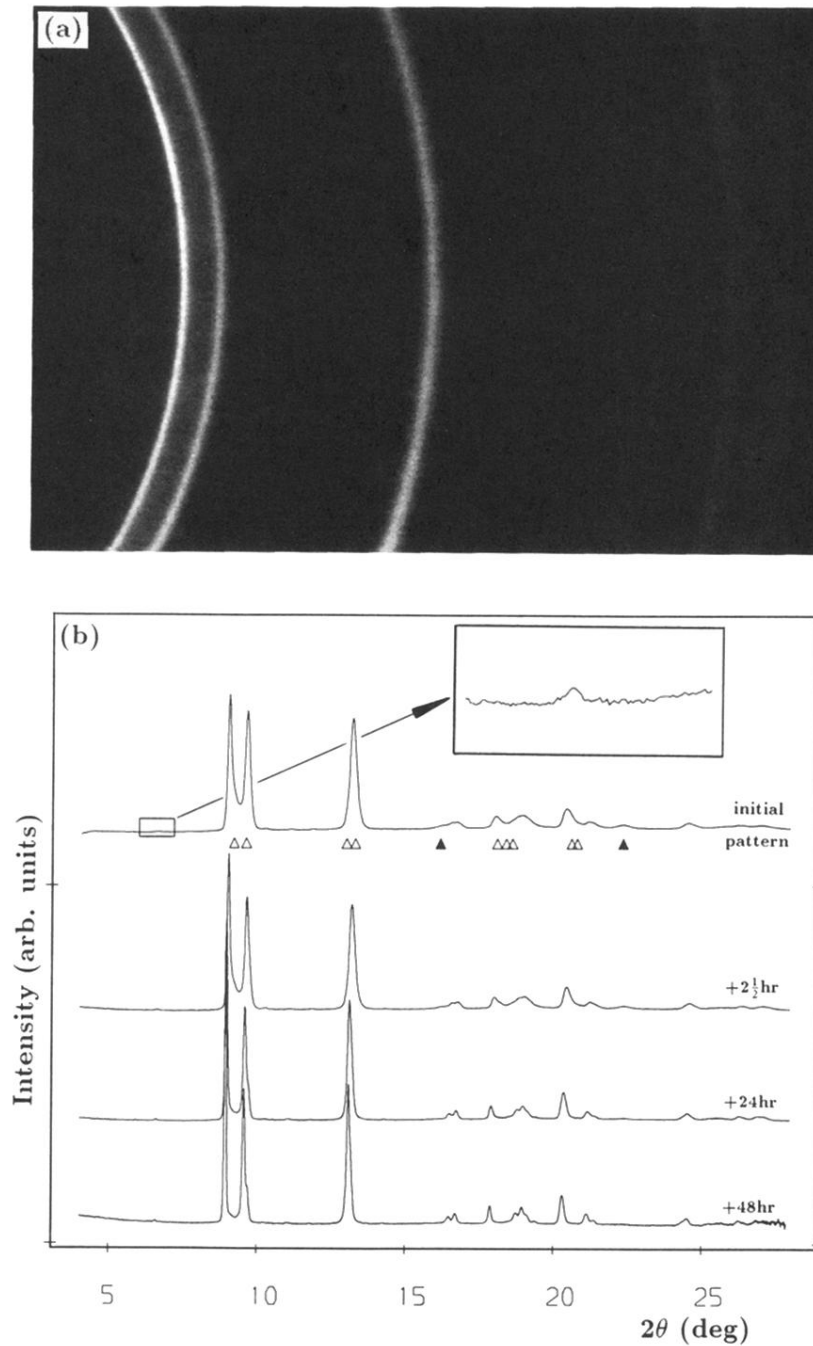FIG. 12. (a) A pattern recorded from InSb at about 2.3 GPa after passing rapidly through the transition. $\lambda = 0.4442$ Å. Exposure time = 51 min. Sample-to-plate distance = 200 mm. (b) The corresponding integrated profile, and its subsequent evolution over a period of 2 days. The triangles under the initial profile show the positions of the principal $\beta$-tin lines. The one marked by a solid triangle at $2\theta \sim 22°$ is the nonoverlapping $P2$ line indicated at the same position in Fig. 4(b). The weak low-angle line is enlarged in the inset.

FIG. 15. (a) A mixed $P3$-$P4$ pattern recorded from InSb after passing through the transition at $\sim 3.0$ GPa. The strongest $P4$ lines are labeled "a," and the single visible $P3$ line is labeled "b." $\lambda = 0.4446$ Å. Exposure time = 26 min. Sample-to-plate distance = 250 mm. (b) A pattern recorded from the same sample 15 h later, after $P3$ has recrystallized to $P4$. $\lambda = 0.4446$ Å. Exposure time = 42 min. Sample-to-plate distance = 250 mm.
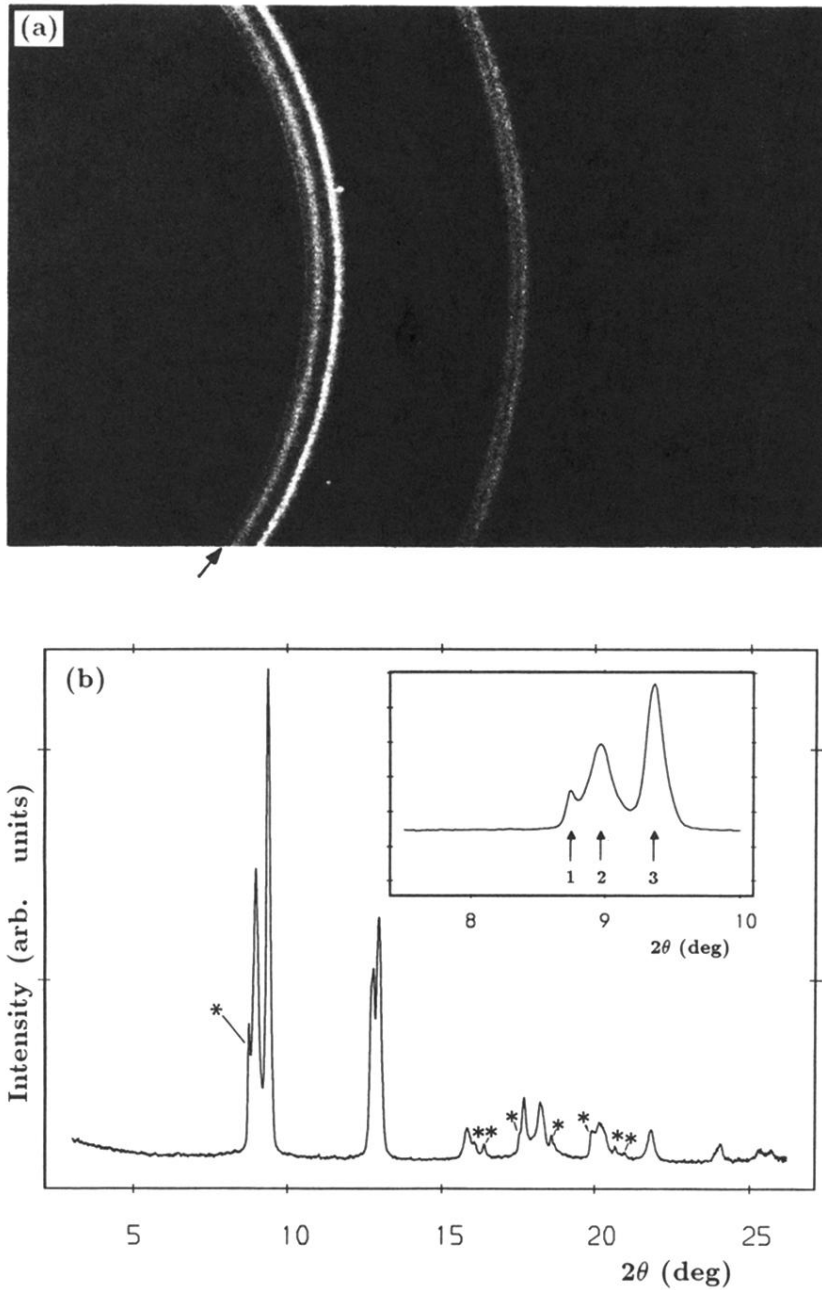
FIG. 3. (a) A pattern recorded from a mixture of InSb P2 and P3 at, or slightly above, the pressure in Fig. 2. The arrow marks the first line of one phase (P3). The adjacent broader lines are the first two of the second phase (P2). λ=0.4442 Å. Exposure time=10 min. Sample-to-plate distance=350 mm. (b) The corresponding integrated profile. The asterisks mark the sharp-peaked features of P3. The inset displays the first three peaks on the same 2θ scale as in the inset of Fig. 2.
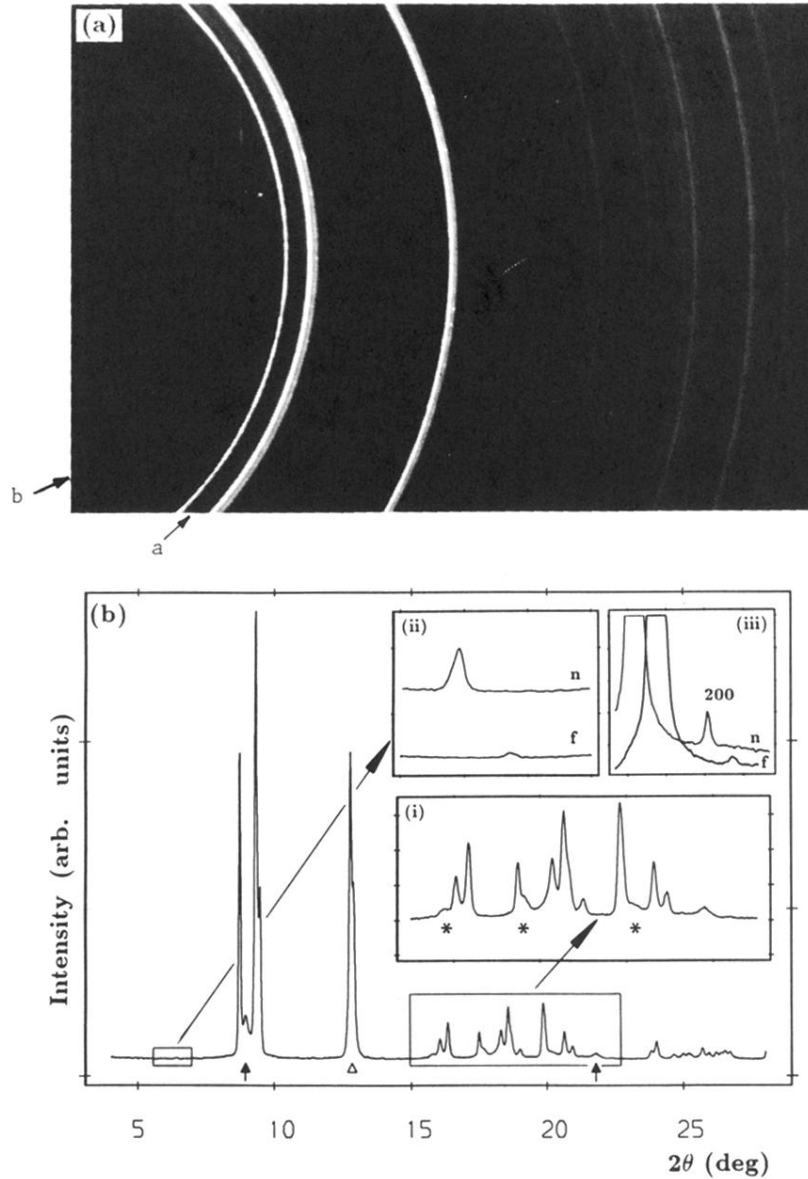
FIG. 4. (a) A pattern recorded from a mixture of InSb $P2$ and $P3$ at, or slightly above, $\sim 2.1$ GPa. The lowest-angle strong line of $P2$ is labeled "a" and the very weak low-angle line of $P3$ is labeled "b." $\lambda = 0.4446$ Å. Exposure time $= 14$ min. Sample-to-plate distance $= 250$ mm. (b) The corresponding integrated profile. The arrows below the profile mark the two nonoverlapped $P2$ lines (the one at $2\theta \sim 9°$ is marked "a" in the 2D pattern). The features marked $\Delta$ and $*$ [inset (i)] are discussed in the text. Inset (ii) shows the very weak low-angle line of $P3$ (marked "b" in the 2D pattern) recorded with an incident energy of 25.83 keV, far ($f$) from the In $K$ edge (as in the main profile), and at 27.886 keV near ($n$) the In $K$ edge (at 27.925 keV). Inset (iii) shows the cubic (200) reflection recorded with the same two incident x-ray energies as for inset (ii).
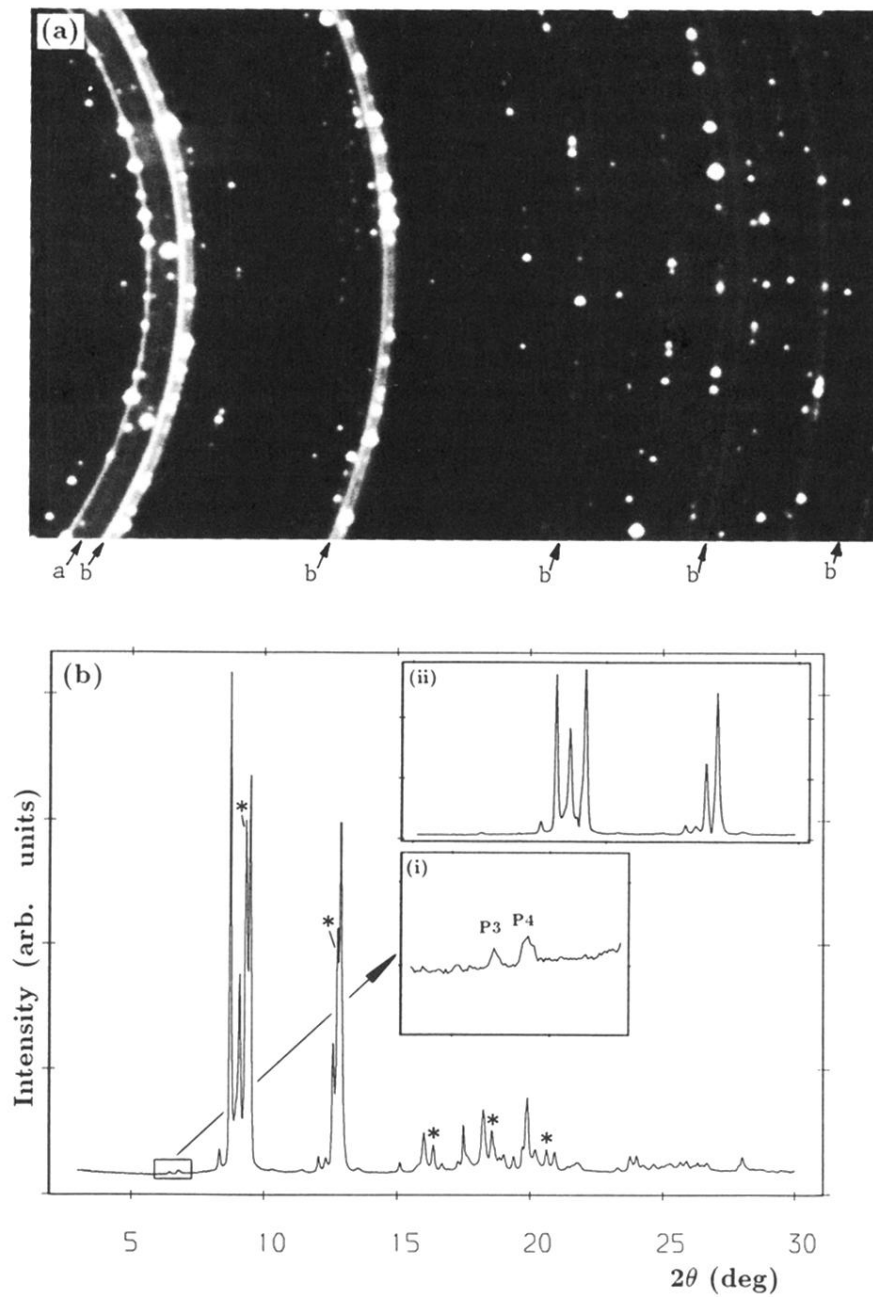
FIG. 6. (a) A pattern recorded from a sample of InSb $P3$ partly transformed to $P4$ just above 2.1 GPa. Some $P2$ is also still present, as shown by the line labeled "a." The $P3$ lines labeled "b" are not overlapped by any $P4$ lines, and hence are free from spots. $\lambda = 0.4446$ Å. Exposure = 10 min. Sample-to-plate distance = 250 mm. (b) The corresponding integrated profile. Asterisks mark the strongest of the nonoverlapped $P3$ lines, labeled "b" in (a). The low-angle weak line of $P3$ is enlarged in inset (i), with a weak $P4$ line alongside. Inset (ii) shows the part of the profile below $2\theta = 15°$, with the best-fitting calculated $P3$ profile subtracted to reveal the main $P4$ lines.
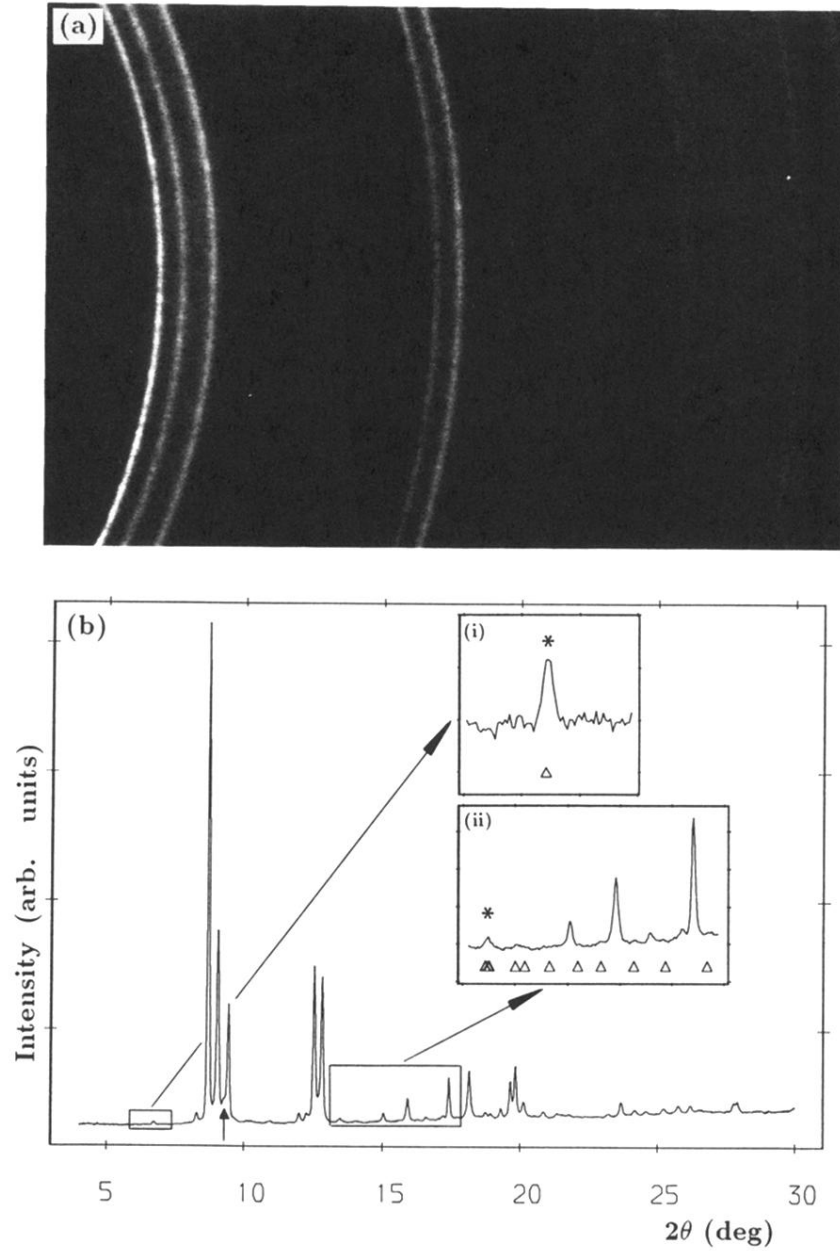
FIG. 8. (a) A pattern recorded from InSb $P4$ at $\sim 3$ GPa, just above the transition directly from the cubic phase. $\lambda = 0.4446$ Å. Exposure time $= 42$ min. Sample-to-plate distance $= 250$ mm. (b) The corresponding integrated profile. The insets show parts of the profile enlarged, as indicated. The arrow below the main profile indicates a weak non-$P4$ line. The marked features in the insets are discussed in the text.
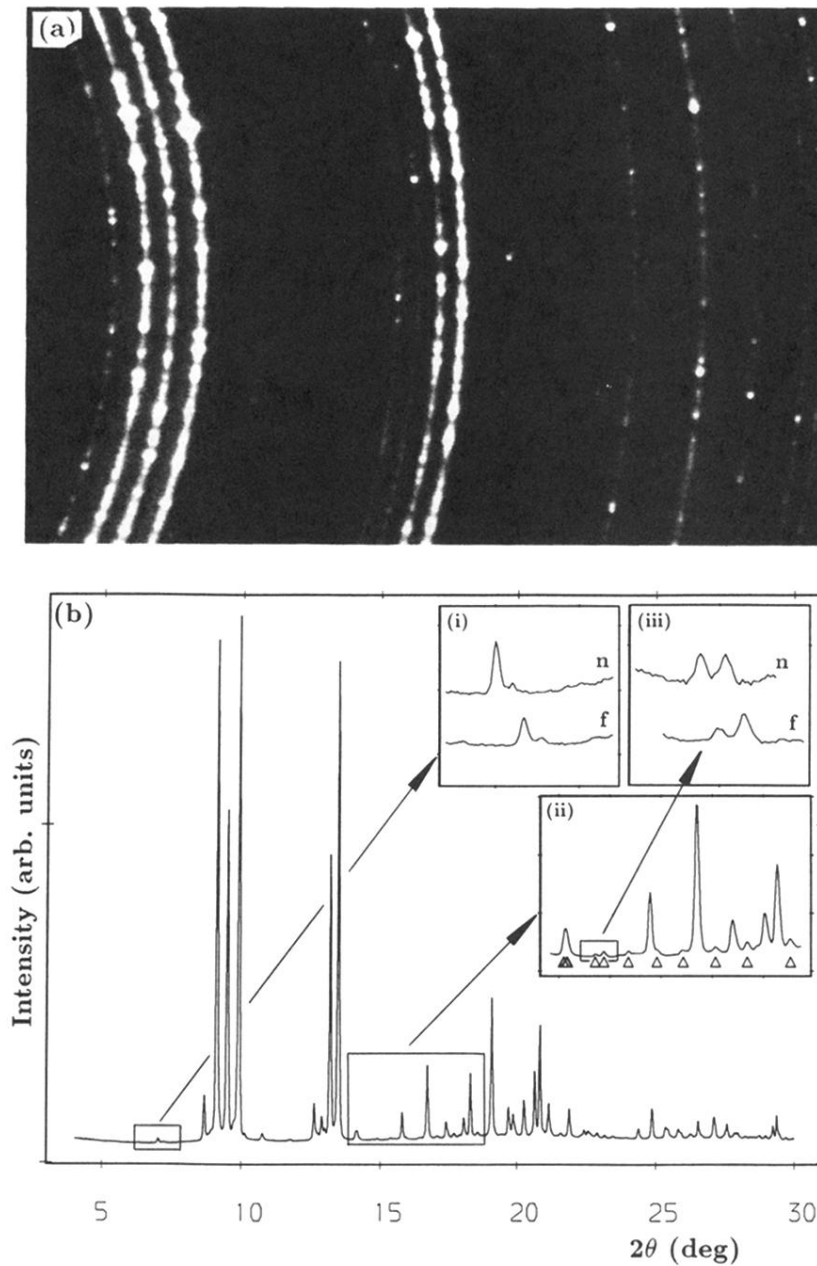
FIG. 9. (a) A pattern recorded from InSb $P4$ at $\sim 2.5$ GPa and 100 °C. $\lambda = 0.4642$ Å. Exposure time = 146 min. Sample-to-plate distance = 250 mm. (b) The corresponding integrated profile. Inset (i) shows a weak low-angle line recorded with an incident x-ray energy of 26.709 keV, far ($f$) from the In $K$ edge (as in the main profile), and at 27.886 keV, near ($n$) the In $K$ edge (at 27.925 keV). The enlargement in inset (ii) reveals many weak superlattice reflections, marked $\Delta$. Two of these are enlarged further in inset (iii), recorded far from and near the In $K$ edge as in (i).